5 Magnetron Sputtering of ZnO Films

B. Szyszka

5.1 Introduction

Glow discharge sputtering is one of the oldest deposition techniques that utilizes an energy input to promote surface diffusion at the substrate and thus, to achieve dense and well-adhering coatings at low substrate temperatures. The term "sputtering" means the ejection of atoms from a usually solid target material due to the impact of highly energetic species. These highly energetic species are usually positive ions, which can either be accelerated in the cathode sheath of a plasma discharge or in an ion source.

The simplest approach for the deposition of ZnO films by sputtering is sketched in Fig. 5.1: A DC glow discharge is ignited between a cathode, which is a planar Zn target, and the anode, which is the chamber of the vacuum system. The system is pumped to a pressure of ∼10 Pa and Ar and O_2 are introduced into the system.

The metallic target is oxidized, so that Zn and O atoms are sputtered from the target and condense on the substrate, where the ZnO film is formed. However, this concept has many drawbacks in terms of film properties, deposition rate, and process stability. The development of the so-called "magnetron" sputter sources by Chapin [1] was a breakthrough in the 1970s toward large area high-rate deposition. The key was to increase the sputter current by magnetic confinement of the plasma in front of the target. This feature allows both the deposition rate to be increased and the pressure to be decreased. Both features are crucial for cost effective sputter deposition of high-quality ZnO films.

For transparent and conductive ZnO-based TCO films, however, several further breakthroughs have been necessary: The most crucial point is the control of stoichiometry and phase composition, which are key parameters for efficient doping. Many approaches have been realized: Reactive sputtering from alloy targets allows growth conditions to be varied to a large extent. The metallic targets used are cheap compared to ceramic targets but the drawback is the need for a precise control of the reactive process, which is a delicate but solvable task using advanced process control techniques. Ceramic target sputtering on the other hand permits more robust processes since the metal-to-oxygen ratio is defined by the target stoichiometry up to a certain extent.

The following sections review the work on magnetron sputtering of ZnO films focusing on TCO properties. Section 5.2 outlines the history of ZnO

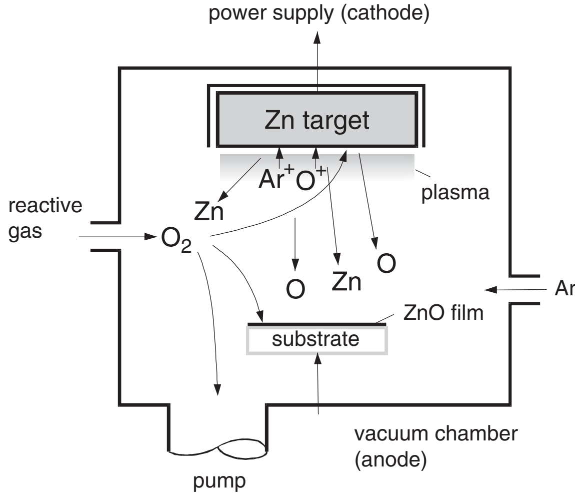

Fig. 5.1. Setup for glow discharge sputter deposition of ZnO by reactive DC sputtering of a metallic Zn target in an Ar/O_2 atmosphere

sputtering. Section 5.3 is about the basics of magnetron sputtering and the ZnO film properties, which can be achieved by magnetron sputtering. Section 5.4 treats the manufacturing technology for large area deposition and Sect. 5.5 gives an overview of emerging developments toward more advanced and lower-cost ZnO sputtering technology.

5.2 History of ZnO Sputtering

Sputtering of ZnO films has a history covering more than three decades. The technique is now one of the most versatile deposition processes for industrial production of ZnO films.

First sputtering processes for ZnO deposition were developed in the late 1960s for manufacturing surface acoustic wave devices [2]. The piezoelectric properties of ZnO films are crucial for that application and major efforts were made to develop ZnO sputtering processes which enabled *c*-axis oriented growth, high resistivity and unique termination of the ZnO crystallites [3,4].

Large-area sputtering of ZnO was established in the field of energy-efficient glazing in the early 1980's. At that time, ZnO was used as a dielectric film for Ag-based low emissive (low-E) coatings. Coating designs such as float glass/ZnO/Ag/blocker/ZnO were implemented by planar cathode reactive sputtering onto large-area glass panes [5,6]. ZnO was chosen as dielectric material because of its high sputtering rate and its suitability for reactive DC sputtering.

Even today, ZnO films are key components in modern Ag-based coatings for architectural glazing. Nowadays, the most challenging application

of ZnO for architectural glazing is its use as a seeding layer for the growth of highly conductive Ag and also as a blocker film on top of the Ag. Two different aspects are important for this application: For the seeding layer, it is the wurtzite phase crystal structure: Appropriately deposited ZnO films reveal *c*-axis oriented textured growth, which promotes the heteroepitaxial growth of Ag. The state of the art is to use a ZnO-based films as thin seeding layer (∼2–5 nm thickness) for the silver film [7, 8]. The use of ZnO films as a nonabsorbing blocker on top of the Ag is enabled by ceramic target magnetron sputtering [9]. Compared to reactive magnetron sputtering, this process allows the particle energy at the surface of the growing film to be decreased significantly, which is crucial to maintaining the metallic conductivity of the Ag film underneath.

Transparent and conductive, sputtered ZnO-based films with resistivity below 1,000 $\mu\Omega$ cm were first reported by Brett and coworkers in the early 1980's [10]. Breakthroughs such as high-rate magnetron sputtering of ZnO:Al [11] guided the developments toward large-area manufacturing technology, with main emphasize on thin-film photovoltaics [12, 13].

5.3 Magnetron Sputtering

Magnetron sputtering [14] is a production proven high precision and high-rate coating technology based on simple and rugged components. The technology was developed in the early 1970's [1]. The first applications were the metallization of polymer parts for the automotive industry, the metallization of wafers for microelectronics [15], and the large-area deposition of energy-efficient coatings for architectural glazing. Further applications are numerous; major examples are coatings on polymeric web [16] and display glass [17, 18], as well as coatings for data storages, such as CD's, DVD's [19] and hard disk drives [20]. Magnetron sputtering is also a key technology for wear-resistant coatings on tools and components. Furthermore, magnetron sputtering processes are essential to the industrial manufacturing of thin-film solar cells, where transparent electrodes and back contacts are deposited by magnetron sputtering and where major R&D efforts are concentrating on the deposition of semiconductors using this technique.

It is a high-vacuum deposition process where the film-forming atoms are generated by sputtering from a metallic or compound target plate, which is the cathode of a glow discharge process. The sputtered atoms are transported to the substrate through a low pressure plasma environment. The condensation of mostly neutral atoms and film growth is under concurrent bombardment by energetic species from the plasma [21], which promotes nucleation, compound formation, and film growth on the substrate [22, 23].

Since the coating material is passed into the vapor phase via momentum exchange caused by energetic particle impact rather than by a chemical or thermal process, virtually any material is a candidate for coating. Films

containing almost every solid element in the periodic table have been prepared by sputtering. Alloys and compounds can be sputtered such their stoichiometry is preserved, so oxide films such as ZnO:Al can be sputtered either reactively from a metallic alloy target, where reactive gas is introduced into the process chamber, or from ceramic compound targets in a pure Ar atmosphere.

The process technology of magnetron sputtering has been described extensively in the literature [24, 25]. A noteworthy introduction into magnetron sputtering of optical coatings is given by Herrmann et al. [26].

5.3.1 Glow Discharge Characteristics

The sputtering target is the cathode of a low pressure glow discharge operating in either in a non-reactive (compound target sputtering in Ar) or reactive atmosphere (elemental target sputtering in Ar/O_2 mixture). High pressure in the order of $5 - 15\,\text{Pa}$ is necessary for sputtering without the support of a magnetic field. The target is subject to an ion bombardment by Ar^+ and O^+ ions, which are generated by electron impact ionization and which are accelerated in the cathode sheath toward the target.

Plasma formation and the characteristics of glow discharge processes are subjects of extensive monographs [27, 28].

5.3.2 Processes at the Target Surface

Sputtering of the target material is the fundamental process for the generation of thin film forming species. Sputtering is a process whereby material is dislodged and ejected from the surface of a solid target material as a result of momentum exchange associated by energetic particle impact. The impact of particles with energy of several 100 eV gives rise to a collision cascade in the target, which ends up in the emission of a certain amount of target atoms at energies of a few electronvolt as neutral atoms mostly. An overview on the processes at the target surface is given in Fig. 5.2.

The properties of the emitted material depend on the bombarding ions, their kinetic energy, incidence angle, atomic mass as well as on the target material and its structure. The most important parameter of the sputtering process is the so-called *sputter yield* Y which defines the number of emitted target atoms Z_{e} per incident particles Z_{i}.

$$Y = \frac{Z_{\mathrm{e}}}{Z_{\mathrm{i}}} \tag{5.1}$$

The dependence of sputtering yield on ion energy is shown in Fig. 5.3 for different elemental targets. At moderate ion energies in the order of 30 to 1,000 eV, sputtering is characterized by *knock on* effects where the incident ions collide with a surface atom and these atoms further react with additional atoms. These events may eventually lead to a release of target material atoms.

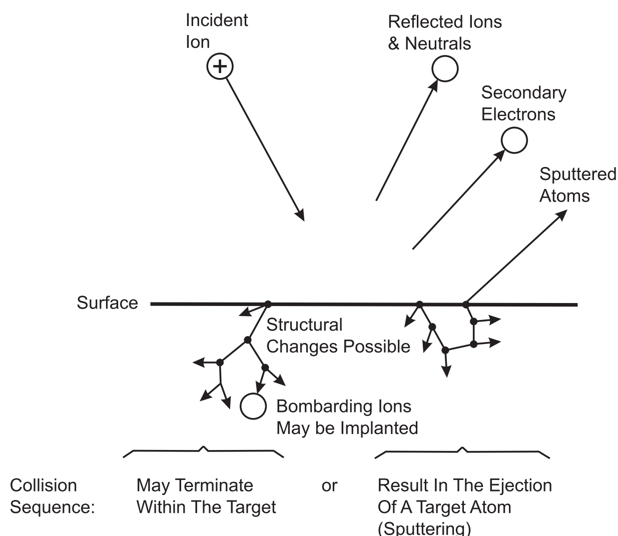

Fig. 5.2. Processes occurring at the target surface due to the impact of highly energetic particles (reprinted from [27])

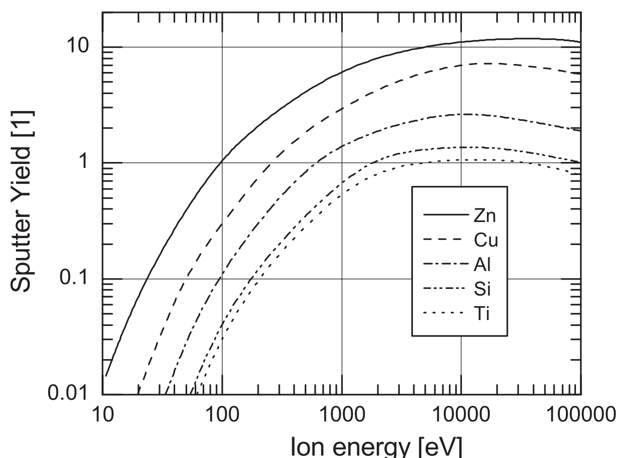

Fig. 5.3. The sputtering yield of Si, Zn, Ti, Cu, and Al for Ar^+ bombardment as a function of ion energy. The sputtering yield for Zn at 300, 500, and 1,000 eV is 3.7, 5, and 7, respectively (reprinted from [30])

In this regime, the sputtering depends strongly on the details of the interaction such as the geometric position of the impinging ions on the target surface and the local binding energies. The sputtering yields and the effect of target poisoning due to oxide formation on the target surface as well as oxide

implantation can be modeled using Monte Carlo simulations implemented in tools such as TRIDYN [29].

At low energy, a threshold is observed. This is due to the fact that the surface binding energy barrier has to be overcome for sputtering to occur. An important consequence is that the sputter yield of an oxidized target surface is much smaller than for a metallic surface.

At high energy, the impinging ion has enough energy to break all bonds in its local environment. This is the *collision cascade regime*, which can be accurately modeled.

For the application of ZnO sputtering using Ar as sputter gas and typical deposition conditions with impinging ion energy in the order of 100–1,000 eV, it is remarkable that Zn has the highest sputtering rate known for any elemental target material.

Further information on the details of the sputtering process can be found in the extensive literature [31, 32].

5.3.3 Magnetron Operation

The conventional configuration for reactive glow discharge sputtering described in Fig. 5.1 suffers from the low ionization efficiency of the electrons crossing the gap between the cathode and the anode. Pressures on the order of 10 Pa are necessary to operate the discharge. The discharge current is small and therefore, the growth rate is low. Furthermore, the high pressure gives rise to an unwanted thermalization of the low-energy sputtered target material atoms. High-energy species, on the other hand, such as fast, reflected Ar neutrals and negatively charged oxygen ions are not thermalized to the same extent, since the scattering cross sections depends strongly on the particle energy [33]. This effect gives rise to an increased defect density in the growing film since the surface diffusion promoting low-energy species with kinetic energy up to a few tenth of electronvolt [34] are suppressed, while the unwanted high-energy and thus defect-generating species with higher energies still reach the substrate. Furthermore, the substrate is subject to intense electron bombardment, causing a substantial heat load which is unwanted in many applications.

These drawbacks can be circumvented using the *magnetron* configuration of the sputtering cathode. Magnetron sputtering utilizes magnetic trapping of the electrons to confine the plasma close to the cathode [25]. The magnetic field is formed parallel to the cathode surface and perpendicular to the electric field, as shown in Fig. 5.4.

As a consequence, the electrons which are accelerated in the cathode sheath are forced onto a closed loop drift path parallel to the target surface because of the Lorentz Force. This magnetic trapping of the electrons and the corresponding ambipolar diffusion of the ions raises the plasma density in front of the target. A much higher ion current and therefore deposition rate is possible. Furthermore, the pressure can be decreased, which improves

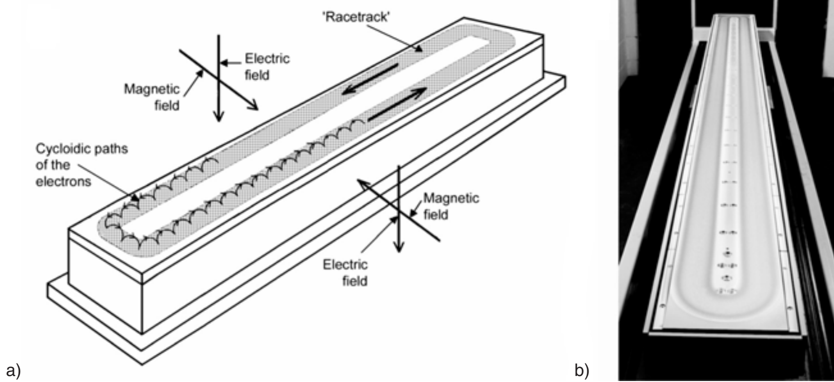

Fig. 5.4. (**a**) Operation principle of a planar magnetron cathode. The secondary electrons emitted from target surface are trapped by the magnetic field due to the Lorentz force. The result is a plasma torus in front of the target. (**b**) Planar magnetron cathode of 3.75 m length (from [35])

the film properties since less scattering in the gas phase occurs. Also, the thermal load on the substrate is decreased. Magnetron sputtering therefore allows for coating on temperature-sensitive substrates, such as polymers or organic coatings.

The plasma discharge can be excited using DC, MF (some tens of kHz) or RF (13.56 MHz) excitation. The positive ions bombard the negatively-charged target electrode which serves as the cathode of the discharge. The first use of such a configuration was reported by Penning et al. for sputtering a cylindrical cathode in a coaxial magnetic field [36, 37]. However, it took more than 30 years for the invention of the planar magnetron by Chapin [1].

The plasma confinement allows low pressure/high current operation of the discharge. The total pressure can be as low as 0.1 Pa. For a target-to-substrate distance in the order of 100 mm, direct transport of target material to the substrate occurs in the line of sight at that low pressure. Interactions of sputtered material with the gas phase are limited to a few collisions. As a consequence, much of the kinetic energy of sputtered material can be transferred to the substrate, enhancing surface diffusion and reactivity and improving the film properties compared to conventional sputtering or evaporation processes.

The energetic bombardment of the substrate can be changed using a variety of modified magnetron sputter processes such as dual magnetron operation with MF plasma excitation [38], RF superimposed DC magnetron sputtering [39] and unbalanced magnetron sputtering [40]. The basic concept of these techniques is to utilize intense low-energy ion bombardment from a dense plasma near the substrate to improve the thin-film properties.

5.3.4 Magnetron Sputtering of ZnO

As outlined in Sect. 5.2, many attempts have been made to deposit ZnO-based films by sputtering. The compilation of papers in Table 5.1 may serve as a reference to identify useful papers. The classification criteria are: plasma excitation used (DC/MF/RF); reactive or ceramic deposition; material deposited and film properties relevant for TCO applications.

5.3.4.1 Reactive Magnetron Sputtering

In reactive magnetron sputtering [66], metal targets are sputtered in a reactive atmosphere. This approach is not only cost-effective due to the use of metal alloys instead of ceramics but also allows the film properties to be varied to a large extent. The fundamental operating principle for reactive sputtering is sketched in Fig. 5.1. The metallic sputter target serves as the cathode of a glow discharge operating in an Ar/O_2 gas mixture and the anode can be considered to be the chamber. However, there are other ways to operate the discharge such as medium frequency (MF) dual magnetron and radio frequency (RF), which are described later on. The target is bombarded by high-energy ions which are accelerated toward the cathode. This process releases metal atoms (Zn) from metallic areas of the targets as well as atomic oxygen (O) from oxidized areas of the target surface. The sputtered material condenses on the substrate, where it reacts with the reactive gas and forms and oxide film.

The reactive sputter process can be considered as a getter pump where the reactive gas is gettered by the reaction with the target material. The pumping speed of this getter pump, however, depends strongly on the state of the target surface since the release of metal atoms by sputtering depends on the sputtering yield. This effect gives rise to the nonlinear process characteristics of reactive magnetron sputtering, as shown in Fig. 5.5 for reactive magnetron sputtering of ZnO:Al films. The discharge is operated at constant power using the reactive MF magnetron sputtering process described in [38]. The discharge voltage and total pressure are shown as a function of the oxygen flow rate.

A continuous dependence of total pressure and discharge voltage on the oxygen flow rate is observed only for low or high oxygen flow rates, whereas an abrupt noncontinuous change of process parameters is observed at intermediate flow rates. Furthermore, strong hysteresis is observed between increasing and decreasing oxygen flow rates. The three process regimes are related to the state of the target. The nomenclature was proposed by Schiller et al. [67]: Elemental or metallic mode, transition mode, and compound or oxide mode.

Metallic Mode

- When the partial pressure of the reactive gas is low, the target surface is metallic or partially oxidized. The target coverage is a continuous function of the oxygen partial pressure.

Table 5.1. Literature survey on magnetron sputtering of ZnO-based TCO films

Ref.	Scope	Growth conditions	Layer properties
	Process Material Goal Year	Coater and magnetron Process mode and control Target Substrate, T_S (°C) P/A (W cm^{-2}) a_s (nm s^{-1})/a_d (nm m min^{-1})	d (nm), c_d (at.%) ρ (Ω cm), n_e (cm^{-3}), μ (cm^2 V^{-1} s^{-1})
[41]	RDCMS ZnO_{1-x} fd 1985	Batch, 150 mm planar Baffle, substrate RF bias Zn Glass, PET, 80°C	700 nm, $x = 0.05$ 1.9×10^{-3} Ω cm, 1.8×10^{20} cm^{-3}, 18 cm^2 V^{-1} s^{-1}
[42]	RDCMS ZnO:Al fd 1999	Batch, 90 mm planar Low power Zn:2 wt% Al Glass, RT 1.6 W cm^{-2}, 0.8 − 2 nm s^{-1}	170–400 nm, 1.4 − 1.8 at.% 6×10^{-4} Ω cm, 1.0×10^{21} cm^{-3}, 10 cm^2 V^{-1} s^{-1}
[40]	RDCMS ZnO:Al ZnO:In fd 1991	Batch Low power Zn target, Al or In pieces Glass, 180 − 220°C <2 nm s^{-1}	700 nm 2 at.% (Al), ∼11 at.% (In) 5.0×10^{-4} Ω cm (Al) 1.4×10^{-3} Ω cm (In)
[11]	RDCMS ZnO:Al fd 1994	Batch, 3 inch planar Low power Zn:2 wt% Al Glass, <150°C 2.2 W cm^{-2} <2 nm s^{-1}	∼500 nm 1.8–2.2 at.% 4.5×10^{-4} Ω cm 8×10^{20} cm^{-3} 17 cm^2 V s^{-1}
[43]	RDCMS, RMFMS ZnO:Al lac, dd 2003	In-line, dual magnetron tm, q(O_2) = f(PEM) 1 400 × 100 mm^2 each Zn:2.0 wt% Al Glass, RT <5W cm^{-2} 125 nm m min^{-1}	1,040 nm, 9.1×10^{-4} Ω cm
[44]	RDCMS ZnO:In fd 1992	Batch, 70 mm planar tm, $q(O_2) = f(U)$ Zn:2.5 at.% In Glass, RT 1.2 nm s^{-1}	∼250 nm, ∼$10^{-2} - 10^{-3}$ Ω cm
[45]	DCMS ZnO_{1-x} dev 1991	Batch, 4 inch planar ZnO, H_2O gas Glass, 300–400°C $I = 500$ mA 0.3–0.6 nm s^{-1} dev a-Si, pav	2,000 nm pav: 1.8×10^{-3} Ω cm

Table 5.1. (continued)

Ref.	Scope	Growth conditions	Layer properties
[46]	DCMS ZnO:Al fd 1990	Batch, 120 mm planar Zn0:2–3 wt% Al_2O_3 Glass, 250°C	300–600 nm 2.7×10^{-4} Ω cm
[47]	DCMS ZnO:Ga fd 1997	Batch, 3 inch planar ZnO:3–10 wt% Ga_2O_3, sintered Glass, 100 − 250°C 1.1 W cm^{-2}	300 nm, 2.2×10^{-4} Ω cm, 9×10^{20} cm^{-3}, 32 cm^2 V^{-1} s^{-1} (5.7 wt% Ga_2O_3, 250°C)
[48]	DCMS ZnO:Ga fd 2002	Batch, ∼80 mm planar Zn:5.7 wt% Ga_2O_3 Gas: Ar, Ne, Kr Glass, RT ∼2 W cm^{-2}, 0.2 − 0.6 nm s^{-1}	∼200 nm
[49]	DCMS ZnO:Sc, ZnO:Y fd 2000	Batch, 150 mm planar ZnO:$Sc_2O_3^*$, ZnO:$Y_2O_3^\dagger$ Glass, 200°C 0.6 W cm^{-2}	∼1,000 nm 2 wt%*, 4 wt%† 3.1×10^{-4} Ω cm*, 7.9×10^{-4} Ω cm†, 6.9×10^{20} cm^{-3*}, 29 cm^2 V^{-1} s^{-1*}
[50]	RMFMS ZnO:Al fd 2001	Batch, dual magnetron, 500×88 mm^2 tm, $P = f(U)$ Zn:1.5 wt% Al Glass, RT*, 250°C† ∼6 W cm^{-2}, 7 nm s^{-1}	500 nm ∼3 at.% 7.5×10^{-4} Ω cm*, 2.5×10^{-4} Ω cm†
[51]	RMFMS ZnO:Al fd 1999	Batch, 500×88 mm^2 DMS Met. mode, Zn desorption Zn:0.9–1.5 wt% Al (segmented) 100°C*, 250°C† ∼10 W cm^{-2} 8.2*, 8.8† nm s^{-1}	∼500 nm 3.6 at.%*, 2.2 at.%† $4.8^*, 3.0^\dagger \times 10^{-4}$ Ω cm $8.6^*, 8.5^\dagger \times 10^{20}$ cm^{-3} $15^*, 25^\dagger$ cm^2 V^{-1} s^{-1}
[52]	RMFMS ZnO:Al lac, dd 2003	In-line, 400×120 mm^2 DMS tm, $q(O_2) = f$(PEM) Zn:1.5 wt% Al RT*, 300°C† 2.9 W cm^{-2}	$\sim 10^*, 4.4^\dagger \times 10^{-4}$ Ω cm 5.8×10^{20} cm$^{-3\dagger}$ 24 cm^2 V^{-1} s$^{-1\dagger}$
[53]	RRFS ZnO:Al fd 1988	Batch, 125 mm planar Zn, Al wires Glass, 100°C 0.01 nm s^{-1}	540 nm 4.9×10^{-4} Ω cm 4.3×10^{20} cm^{-3}, 24 cm^2 V^{-1} s^{-1}

Table 5.1. (continued)

Ref.	Scope	Growth conditions	Layer properties
[54]	RFMS ZnO_{1-x} G: fd 1981	Batch, 4 inch planar ZnO, H_2 gas RT−150°C $\sim$1.2 W cm^{-2}, $\sim$0.5 nm s^{-1}	$\sim$1,000 nm 7×10^{-3} Ω cm 1.1×10^{20} cm^{-3}, 8 cm^2 V^{-1} s^{-1} 2×10^{-3} Ω cm: 2nd plasma at substrate
[55]	RFMS ZnO_{1-x} fd 1982	Batch[c)], 80 mm planar ZnO Glass, $\sim$90°C <0.3 nm s^{-1}	200 nm 5×10^{-4} Ω cm 1.0×10^{20} cm^{-3}, 120 cm^2 V^{-1} s^{-1}
[56]	RFS ZnO_{1-x} fd 1983	Batch, 75 mm planar ZnO $\sim$100°C, $\sim$1.4 W cm^{-2},	500 nm 5×10^{-3} Ω cm
[57]	RFMS ZnO:Al fd 1991	Batch, 125 mm magnetron ZnO:2.0 wt% Al_2O_3 Sapphire, 230°C, <1.4 W cm^{-2}, 0.5 nm s^{-1} Hetero epitaxial growth	380–670 nm 2 at.% 1.2 nm min^{-1}: 140 μΩ cm 1.3×10^{21} cm^{-3}, 34 cm^2 V^{-1} s^{-1} 22.3 nm min^{-1}: 300 μΩ cm
[58]	RFMS ZnO:Al fd 1996	Batch, 4 inch planar ZnO:2.0 wt% Al_2O_3 sintered Glass, 150°C	$\sim$700 nm 6.9×10^{-4} Ω cm
[59]	RFMS ZnO:X fd 1996	Batch, 1 inch planar ZnO:2.5 wt% Al_2O_3* ZnO:6.9 wt% Ga_2O_3† ZnO:10.5 wt% In_2O_3‡ 150°C, 11 W cm^{-2}, 0.15 nm s^{-1}	400 − 800 nm, 2.6*, 4.0†, 4.2‡ at.% 8.3*, 5.6†, 9.1‡ $\times 10^{-4}$ Ω cm 3.4*, 5.5†, 5.7‡ $\times 10^{20}$ cm^{-3} 22*, 20†, 12‡ cm^2 V^{-1} s^{-1}
[60]	RFMS ZnO:X fd 1985	Batch, 80 mm planar[b] ZnO* ZnO:B_2O_3† ZnO:Al_2O_3‡ ZnO:Ga_2O_3× ZnO:In_2O_3° Glass, <150°C 2 W cm^{-2}, 0.5 nm s^{-1} su	425–650 nm 3.2*, 6.4†, 1.9‡, 5.1×, 8.1° $\times 10^{-4}$ Ω cm 0.51*, 2.5†, 15‡, 4.4×, 4.0° $\times 10^{20}$ cm^{-3} 38*, 39†, 22‡, 28×, 20° cm^2 V^{-1} s^{-1}
[61]	RFMS ZnO:Al fd 1997	Batch, 4 in. planar ZnO:0.5 wt% Al_2O_3, sintered Glass, 150°C	140 nm 4.7×10^{-4} Ω cm, 7.5×10^{20} cm^{-3}, 15 cm^2 V^{-1} s^{-1}
[62]	RFMS ZnO:(Al, H) fd 1999	Batch ZnO:2.0 wt% Al_2O_3, sintered RT, 2 W cm^{-2}	500 nm 4×10^{-4} Ω cm, 6×10^{20} cm^{-3}, 27 cm^2 V^{-1} s^{-1}

Table 5.1. (continued)

Ref.	Scope	Growth conditions	Layer properties
[63]	RFMS ZnO:Al CIS superstrate, pa 550°C 2001	Batch, 100 mm magnetron ZnO:2.0 wt% Al_2O_3 200–250°C, 3.2 W cm^{-2}, 0.5 nm s^{-1}	$\sim 10^{-3}$ Ω cm
[39]	RFDCMS M: ZnO:Al fd 1998	Batch, 3 inch magnetron ZnO:2.0 wt% Al_2O_3 RT 0.5 W cm^{-2}, <0.5 nm s^{-1} dev CIS	10–370 nm 3.3–4.0 at.% $\sim 7 \times 10^{-4}$ Ω cm, $5–7 \times 10^{20}$ cm^{-3}, ~ 15 cm^2 V^{-1} s^{-1}
[64]	RFMS ZnO:Ga fd 1990	Batch, 126 mm planar ZnO:5.0 wt% Ga_2O_3 Glass, RT, 0.9 W cm^{-2}, 0.1 nm s^{-1}	300 nm $\sim 10^{-3}$ Ω cm, 1.5×10^{21} cm^{-3}, 7–20 cm^2 V^{-1} s^{-1}
[65]	Co-deposition ZnO:Al energy eff. windows 1988	Batch Zn:2 wt% Al Glass, <100°C 0.2 nm s^{-1}	~ 300 nm 2.14 at.% 5.4×10^{-4} Ω cm, 4.5×10^{20} cm^{-3}, 26 cm^2 V^{-1} s^{-1}

(Process (DCMS: DC magnetron sputtering from a ceramic target; RDCMS: reactive DC magnetron sputtering; RMFMS: reactive MF magnetron sputtering; RFMS: RF magnetron sputtering from a ceramic target; RRFMS: reactive RF magnetron sputtering)); (Goal (fd: fundamental development; dev: device-specific; lac: large-area coating; dd: dynamic deposition)); (Remarks (su: substrates perpendicular to the target (otherwise parallel); hetero-epitaxial growth; pav, post-annealed in vacuum; dev a-Si, TCO front electrode for a-Si:H solar cells; dev CIS, TCO front electrode for chalcopyrite solar cells))

– The deposition rate is high because of the high sputter yield of the metallic target surface.
– The deposited films are usually metal-rich and thus absorbing and not suitable for optical applications.
– In the metallic mode, the pumping speed of the sputter process is high compared to the pumping speed of the turbo pump while the opposite is true in the oxide mode. These changes of the systems pumping speed due to target oxidation are even more severe in production systems.

Oxide Mode

– When the oxygen partial pressure is raised to a critical value, the process becomes unstable: An avalanche effect occurs since the rise in oxygen partial pressure decreases the pumping speed for the reactive gas. The target surface becomes fully oxidized.

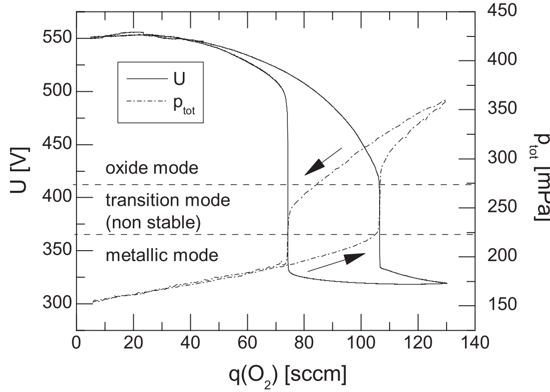

Fig. 5.5. Hysteresis curve for total pressure ($p_{\text{tot}} = p(\text{Ar}) + p(\text{O}_2)$ and target voltage U as a function of oxygen flow $q(\text{O}_2)$ for reactive MF magnetron sputtering of ZnO:Al at constant power, $P = 4\,\text{kW}$. The effective pumping speed of the turbo pump is $380\,\text{l}\,\text{s}^{-1}$, the effective pumping speed of the sputter process for reactive gas is $1{,}230\,\text{l}\,\text{s}^{-1}$ in the metallic mode and $200\,\text{l}\,\text{s}^{-1}$ in the oxide mode (Ar flow $q(\text{Ar}) = 60\,\text{sccm}$). The labeling of the process modes refers to the increase of the oxygen flow (reprinted from [68])

- The deposition rate is low because of the small sputter yield of the compound surface.
- Film growth is under oxygen-rich conditions so the films are stoichiometric. The high partial pressure of the reactive gas limits the surface mobility, so film properties are not ideal. Furthermore, dopants are oxidized and thus, TCO films become non-conductive.
- When the oxygen partial pressure is decreased to a critical limit, the cathode surface becomes partially metallic. The sputter yield is increased and the 2nd avalanche effect occurs for the transition from the oxide to the metallic mode.

Transition Mode

- The transition mode is an unstable process regime for conventional deposition systems. Closed-loop control concepts or modified chamber designs outlined in Sect. 5.3.4.2 are necessary for transition mode process control.
- In transition mode, the oxygen to metal ratio on the substrate is a continuous function of the oxygen partial pressure. It is, therefore, possible to control the stoichiometry of film and thus to optimize doping, morphology, and phase composition.

The non-continuous change of reactive gas partial pressure is the *primary* problem in reactive sputtering of ZnO-based TCO's. The hysteresis characteristics of the reactive process can be modeled within the framework of the *Berg model*, where the condensation of reactive gas atoms on the surfaces

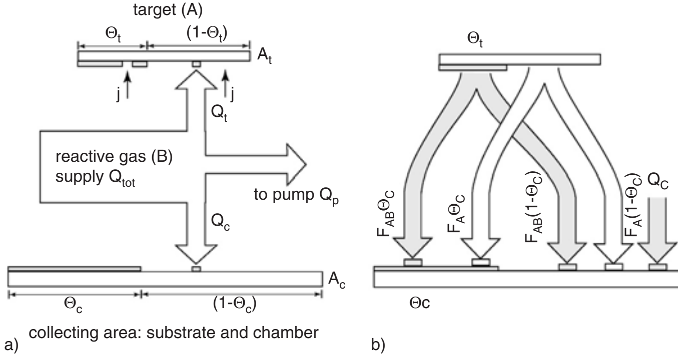

Fig. 5.6. Reactive sputter process for depositing the compound film AB. (**a**) Balance of reactive gas flow Q_{tot}, which is partially gettered at the target (Q_{T}) and at the substrate (Q_{C}) and partially pumped by the vacuum pump (Q_{P}). The fraction of the target surface A_{t} that is covered by the compound AB is Θ_{t}. The fraction of the collecting area A_{c} covered is Θ_{c}. j is the sputter current density. (**b**) Definition of particle fluxes that alter the target and collecting area coverage fractions Θ_{t} and Θ_{c} (see text), (modified from [70])

of the target and chamber and the corresponding changes of pumping speed and sputter yield are taken into account [69, 70]. The basic concept of that model is shown in Fig. 5.6.

Within the framework of the Berg model, the reactive process is described as a gettering process operating on two surfaces, the target and the substrate (including the chamber). Those areas of substrate and target, which are metallic, getter the impinging reactive gas and turn therefore to an oxidized state. The target is sputtered with the ion current of the discharge. The oxidized areas of the target change to a metallic state due to sputtering. At the substrate, by contrast, a change from the oxidized to the metallic state is only possible due to the impinging metal flux from the target.

This simple approach allows the balance equation for the reactive gas partial pressure and deposition rate to be formulated. An example is given in Fig. 5.7 for the stability analysis of process control loops.

The *second* problem is the decrease of the deposition rate in the oxide mode, which is most significant for highly reactive oxides such as MgO and TiO_2, where the deposition rate changes by more than one order of magnitude [72, 73]. For ZnO on the other hand, the deposition rate decreases only by a factor of 2, as shown in Sect. 5.3.4.3.

The *third* problem is process stability at high power levels during long-term operation: In DC operation, the oxidized area of the target is subject to continuous ion bombardment. The oxidized surface exhibits some conductivity, which allows for charge neutralization to a certain extent. When the power is increased further, the dielectrics charge up until the electrical field

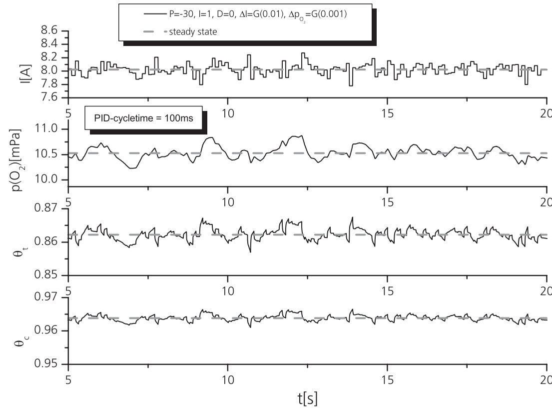

Fig. 5.7. Stability analysis of a process control loop for the reactive magnetron sputtering of high-index metal oxides. The control of discharge power to stabilize the oxygen partial pressure set point is modeled within the framework of the Berg model. A cycle time of 100 ms and process uncertainties for discharge current and oxygen partial pressure measurements are assumed. (from [71])

strength for dielectric breakdown is reached. The stored electric energy is finally transferred into an arc discharge.

Arcs can be either micro-arcs when the surface charge of a small area of the target is transferred into an arc or hard arcs when an arc is ignited between the cathode and ground potential. Micro-arcs may develop rapidly into hard arcs if the power supply is not appropriately controlled. Even micro-arcs give rise to pinhole defects because of local target melting while hard arcs may also damage the target substantially. Arcing is therefore highly undesired in reactive sputtering. Advanced power supplies offer fast arc handling features whereby the discharge power is interrupted when arcing is detected from the current–voltage characteristic of the discharge. Fast arc handling and thus low arc energy is, therefore, an important criterion for choosing a power supply for reactive sputtering [74].

Pulsed plasma excitation instead of DC operation of the discharge opens up further opportunities for stable long-term processes at high power levels. In single magnetron pulse mode deposition, the discharge voltage can either be switched off during pulsing (unipolar pulsing) or the discharge voltage can be applied as a reverse voltage to the target (bipolar pulsing). In bipolar pulsing, the positive charged area is neutralized by the electrons accelerated to the cathode in the afterglow of the plasma discharge. Pulsed operation allows charge neutralization of the target surface and thus prevents the formation of arcs.

A further effect of bipolar pulsed power plasma excitation addresses the disappearing anode effect and thus the long-term stability of reactive sputtering. In conventional reactive DC magnetron operation, the anode gets coated with oxide films. These insulating films give rise to plasma fluctuations

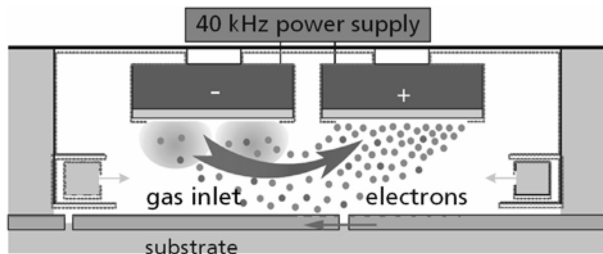

Fig. 5.8. Schematic diagram of the reactive dual magnetron sputter process using MF plasma excitation. $p_{\text{tot}} = 10^{-3} - 10^{-2}$ mbar. Cathode length up to 3.75 m, power density up to 20 W cm^{-2}, plasma excitation frequency 10–100 kHz

since the current path in the plasma is subject to changes which end up in inhomogeneous, non-reproducible coating conditions. This problem is most severe for highly insulating dielectrics such as SiO_2 and MgO but is also relevant for ZnO deposition. The method of choice is dual magnetron sputtering, where two magnetrons operate side by side, connected to a medium frequency (some tenths of kilohertz) power supply, as shown in Fig. 5.8.

One target serves as the anode of the process, while the other target is the actual cathode. The cathode is subject to sputtering and thus, dielectric areas may charge up. The anode, however, is subject to electron bombardment and thus, positive surfaces charges are neutralized in anode operation. Calculations reveal [75] that plasma excitation with a few tenths of kilohertz is sufficient to prevent the dielectric breakdown of these charged surfaces and thus, stable long-term processes can be achieved with a very low arc level. As a consequence, MF plasma excitation allows for higher power levels because of the superior process stability and also improved film properties because of the more intense ion bombardment of the substrate [38].

Reactive MF magnetron sputtering was developed in the early 1990's. Today, it is the state-of-the-art production technology for large-area optical coatings [76] and beside ceramic target magnetron sputtering a promising candidate for the mass production of ZnO-based TCO's by sputtering for thin-film photovoltaics.

5.3.4.2 Control of Stoichiometry and Phase Composition

The properties of ZnO films depend strongly on stoichiometry and phase composition. This holds for TCO films as well as for dielectric films:

Dielectric ZnO Films

– For ZnO films with good piezoelectric properties, it is crucial to achieve c-axis oriented growth as well as a unique termination of the wurtzite phase ZnO crystallites [3].

TCO Films Based on Substoichiometric ZnO

- n-doping can be achieved for substoichiometric ZnO films where two electrons are generated for each oxygen vacancy. ZnO_{1-x} films with $x < 0.05$ exhibit small absorption in the visible range as well as a carrier density up to $2 \times 10^{20}\,cm^{-3}$ [41].
- Substoichiometric films can be obtained either by substoichiometric growth conditions [10] or by subsequent reduction. Annealing in H_2 atmosphere decreases the resistivity considerably for ZnO films deposited by spray pyrolysis [77]. Sputtered ZnO:Al films do not show a substantial effect [78].

TCO Films Based on Doped ZnO

- Doping by group III elements allows for the substitution of Zn and thus, for the creation of one electron per dopant atom.
- TCO films such as ZnO:Al, ZnO:In, and ZnO:Ga are meta-stable materials since the phase segregation (e.g., formation of the oxides of the dopants instead of substitutional incorporation) is favored by thermodynamics. The doping efficiency for magnetron sputtered ZnO:Al films is usually below 50%. Doping efficiency up to 100% has been reported for films by PLD [79].
- Hydrogen doping is another method for n-doping of ZnO [80]. The incorporation of hydrogen is on interstitials. First principle simulations reveal that hydrogen is bonded to oxygen atoms as H^+, contributing one electron to the conduction band [81].

To summarize, it is mandatory to achieve growth conditions where the metal-to-oxygen ratio at the substrate is sufficient not only for transparent film formation but also for appropriate doping.

In reactive magnetron sputtering, the technical implementation of high doping efficiency is difficult due to the hysteresis problem described earlier. The most important deposition parameters for reactive deposition are (1) the rate and the composition of the sputtered material at the target, (2) oxygen partial pressure $p(O_2)$, (3) total pressure p_{tot}, (4) and substrate temperature T_S. Optimization of these parameters is a difficult task, which is still a burden for broad use of that technology: The core problem in reactive sputtering of not only ZnO but also for other compounds is the strong coupling of growth processes at the substrate with the oxidization state of the target material.

There are several approaches to solve this particular problem:

- Baffling of the cathode
- Separation of the gas inlets for the sputtering and reactive gases
- Desorption of surplus zinc
- Separation of deposition and reaction zones
- Transition mode process control

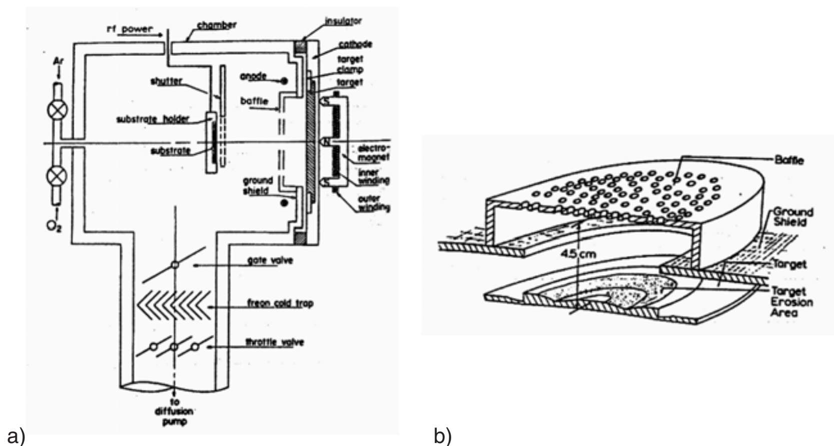

Fig. 5.9. Configuration for a baffled reactive magnetron used by Brett et al. for growing substoichiometric transparent and conductive ZnO films. (**a**) Schematic diagram of the coater. (**b**) reactive gas baffle used for metallic mode ZnO deposition (reprinted from [10])

An overview of these topics is given in [26] for optical films in general. The following subsections refer to ZnO deposition in more detail, taking also the specific property of Zn, its extraordinarily high vapor pressure, into account.

In ceramic target sputtering, by contrast, the situation is not as difficult since the most important parameter, the metal-to-oxygen ratio, is defined by the stoichiometry of the ceramic target material to a certain extent. Ceramic target sputtering is described in Sect. 5.3.5.

Metallic Mode Sputtering Using Baffles

The use of a baffle between the target and the substrate creates a reactive gas partial pressure gradient when the reactive gas is introduced near the substrate. In this way, the cathode can be operated in the metallic mode even with a high reactive gas partial pressure at the substrate.

The concept of baffled reactive magnetron sputtering dates back to the early 1980s [10]. The basic configuration is shown in Fig. 5.9. A reactive gas baffle is mounted in front of the target.

Furthermore, RF biasing of the substrate has been used to achieve desorption of surplus Zn activated by energetic bombardment from the RF discharge at the substrate. This technology allows for fine tuning of the stoichiometry. Transparent substoichiometric ZnO_{1-x} films with $x = 0.01$ were grown with $n_e = 1.6 \times 10^{20}\,cm^{-3}$ and $\mu = 19\,cm^2\,V^{-1}\,s^{-1}$ corresponding to $\rho = 2.1 \times 10^{-3}\,\Omega\,cm$.

A similar technology has also been reported by Maniv et al. [82] using RF biased substrate rotation and larger magnetrons. The lowest resistivity

achieved was $2 \times 10^{-2}\,\Omega\,\mathrm{cm}$ in this case because of the inferior stoichiometry control using a large-area deposition system.

A comparison of the influence of the substrate potential on Zn desorption during reactive DC magnetron sputtering of ZnO:Al has been given by Wendt et al. [83]. ZnO:Al deposition on floating substrates revealed substoichiometric growth, while films deposited on conductive substrates kept at ground potential were fully oxidized. Stoichiometry analysis by Rutherford back scattering (RBS) revealed a substantial increase of Al content by a factor up to 4 due to desorption of Zn. The effect is attributed to the higher electron flux for the substrates at ground potential.

The disadvantages of baffled sputter processes are the substantial decrease in deposition rate and the poor long-term stability of the process because of severe flaking by material deposited on the baffle.

Metallic Mode Sputtering Using Zn Desorption

The high vapor pressure of Zn allows even metallic mode operation without reactive gas baffling since desorption of surplus Zn can be achieved by sufficient substrate heating. The feasibility of this approach has been shown using high-rate reactive MF sputtering for ZnO:Al films with a resistivity of $300\,\mu\Omega\,\mathrm{cm}$ at a growth rate of $9\,\mathrm{nm\,s^{-1}}$. The process parameters are summarized in Table 5.2 [51].

Table 5.2. Process parameters for reactive MF magnetron sputtering of ZnO:Al films in the metallic mode using Zn desorption

Process	Reactive MF magnetron sputtering. Sinusoidal plasma excitation (40 kHz, Advanced Energy PEII). Static deposition. Boxcoater Pfeiffer PLS 580. Process operation in the metallic mode of the discharge.		
System parameters	Target–substrate distance	d_{ST}	90 mm
	Target dimensions		$480 \times 88\,\mathrm{mm}^2$
	Target material		A: segmented targets 0.9 – 1.5 wt% Al B: homogenous targets 1.5 and 2.0 wt% Al
	Ar flow	$q(\mathrm{Ar})$	60 sccm
	O_2 flow	$q(O_2)$	A: 163 sccm B: 140 sccm
	Substrate temperature	T_S	A: 200°C B: RT – 300°C
Process parameters	Discharge power	P	8 kW
	Ar partial pressure	$p(\mathrm{Ar})$	150 mPa
	Process control	–	–
	Substrate material	borosilicate glass AF45, Si	
	Deposition rate	a_s	$\sim 9\,\mathrm{nm\,s^{-1}}$
	Film thickness	d	∼500 nm

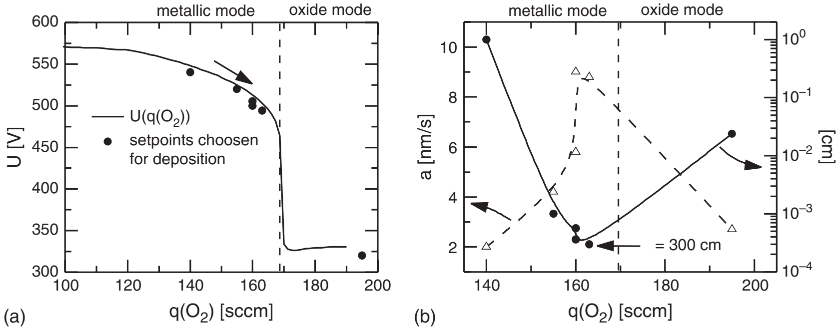

Fig. 5.10. Influence of oxygen flow $q(O_2)$ on target voltage U (**a**) and on deposition rate a and resistivity ρ, respectively, (**b**) for reactive MF magnetron sputtering of ZnO:Al at $T_S = 200°$C. Segmented targets were used (Zn:0.9–1.5 wt% Al). Results shown are for Zn:1.5 wt% Al (reprinted from [51])

Transparent films have been achieved at substrate temperatures exceeding 100°C. The dependence of discharge voltage, deposition rate, and resistivity for deposition at a substrate temperature of $T_S = 200$°C on the oxygen flow rate is shown in Fig. 5.10. Stable operation of the discharge has been achieved in metallic mode for oxygen flow up to 165 sccm. A low deposition rate and high resistivity has been observed at low oxygen flow rates due to the formation of Al-rich films giving rise to Al_2O_3 segregation. An increase of the deposition rate from 2 to 9 nm s^{-1} was achieved when the oxygen flow was raised from 140 to 163 sccm. These films exhibit a low resistivity of $\rho = 300\,\mu\Omega$ cm. Films grown in the oxide mode reveal high resistivity because Al dopants are oxidized under these conditions.

The drawback of this concept is the severe contamination of the coating equipment because of desorption of surplus Zn that condenses on all low-temperature interior surfaces of the coater. Furthermore, the Al doping level increases when the substrate temperature is raised since the highly reactive Al does not desorb. This is shown in Fig. 5.11 where the dependence of the elemental composition on substrate temperature is shown. The Al doping level corresponding to the Al alloy of the targets is 2.1 at.%. However, the observed Al concentration is more than 5 at.% for films deposited at $T_S =$ 300°C. Even at 100°C, the Al concentration is 3.5 at.%. This effect allows transparent ZnO:Al films to be deposited at a low substrate temperature. A resistivity of 480 $\mu\Omega$ cm has been achieved at $T_S = 100$°C.

Transition Mode Process Control

The processing techniques outlined earlier utilize either Zn desorption in the metallic mode or reactive gas partial pressure gradients for the deposition of transparent and conductive ZnO films. From a manufacturing viewpoint,

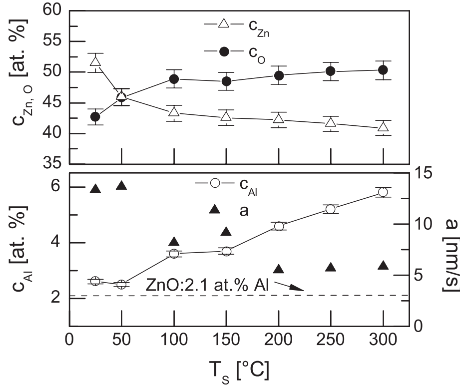

Fig. 5.11. Dependence of Zn, Al, and O content of the ZnO:Al films and deposition rate a on substrate temperature T_S for metallic mode deposition of ZnO:Al (Process parameter set "B" in Table 5.2). The Al concentration without Zn desorption would be 2.1 at.% (reprinted from [51])

these are non-ideal conditions due to the severe reduction in deposition rate and equipment contamination.

Therefore, considerable efforts were made on deposition in the transition mode of the reactive magnetron discharge, where nonstable conditions are used and where closed-loop feedback control is mandatory for process stabilization.

Figure 5.12 gives an overview of some process control techniques that are applicable for the stabilization of reactive sputter processes in the transition mode. The simplest approach to determine the state of a Zn:Al target in reactive sputtering is the measurement of the target voltage, since the plasma impedance decreases when the target is oxidized, as shown in Fig. 5.10. However, the discharge voltage is subject to changes when target erosion or substrate movement occurs. Therefore, more advanced techniques have been developed, such as plasma emission monitoring (PEM) via optical emission spectroscopy or monitoring the oxygen partial pressure via λ-sensors. The controlled variable of the process can be the discharge power or the reactive gas flow.

Other techniques utilize the harmonic analysis of the electrical signal waveforms to determine the target state [84]. Furthermore, the optical properties of films can be measured using in-situ photometry and in-situ ellipsometry for process control [85]. A comparison of the different technologies for transition mode process control is given in [86, 87]. Large-area coaters are usually equipped with either plasma emission monitoring (PEM) of the target coverage to control the oxygen flow [88] or measurement of the oxygen partial pressure to control the discharge power using the λ-probe adapted from the automotive industry [89].

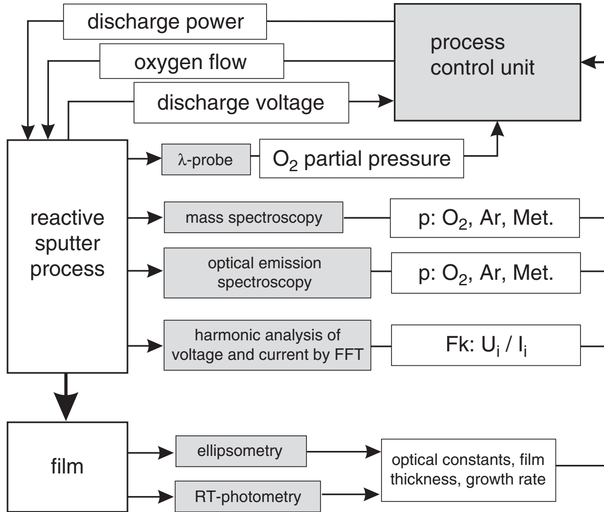

Fig. 5.12. Process control techniques for the in situ characterization of film and process properties and closed-loop control strategies for optical film deposition by reactive sputtering

5.3.4.3 Reactive MF Magnetron Sputtering of ZnO

This section is on the reactive MF magnetron sputtering of ZnO films in the transition mode. The first part is on the deposition of dielectric ZnO films. The reactive sputtering of ZnO:Al is discussed in subsequent sections.

Dielectric Films

Figure 5.13 shows the dependence of O_2 partial pressure on discharge power and the growth rate achieved for ZnO deposition at different substrate temperatures using reactive MF magnetron sputtering. The O_2 partial pressure was measured with a λ-probe and the discharge power was controlled at constant gas flow. The experimental conditions are summarized in Table 5.3.

In Fig. 5.13a at high power (point A) a low O_2 partial pressure of $p(O_2) =$ 10 mPa is achieved. The decrease in discharge power (transition from A to B) shows a continuous increase in reactive gas partial pressure. Beyond point B, a further continuous increase in reactive gas partial pressure can be achieved only by increasing the discharge power. An abrupt transition from the metallic to the oxide mode (point D) would be observed for a further decrease of discharge power.

The closed loop process control permits the process to be stabilized in the region of the unstable *transition mode* between B and C, allowing compensation for the dynamic behavior of the target oxidation by corresponding

control of the discharge power. The scattering of the characteristic curve in Fig. 5.13 indicates the power changes that occur to stabilize the unstable operating points. The symbols indicate the process parameters with which samples were prepared at different substrate temperatures.

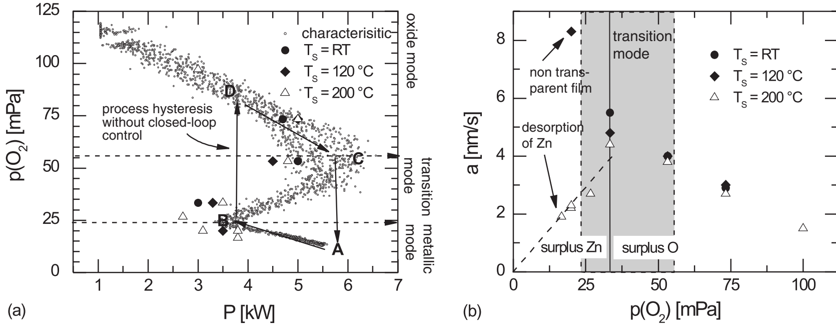

Fig. 5.13. (**a**) Process characteristic for reactive MF magnetron sputtering of ZnO showing the dependence of reactive gas partial pressure $p(O_2)$ on discharge power P and process set points chosen for deposition, (**b**) dependence of growth rate a on reactive gas partial pressure $p(O_2)$ for different substrate temperatures (reprinted from [90])

Table 5.3. Process parameters for reactive MF magnetron sputtering of ZnO films (from [90])

Process	Reactive MF magnetron sputtering. Sinusoidal plasma excitation (40 kHz, advanced energy PEII) Static deposition. Boxcoater Pfeiffer PLS 580. Transition mode process control via λ–probe measurement of O_2-partial pressure.		
System parameter	Target–substrate distance	d_{ST}	90 mm
	Target dimension		$480 \times 88\,mm^2$
	Target material		Zn 99.99 % purity
	Ar flow	$q(Ar)$	2×30 sccm
	O_2 flow	$q(O_2)$	2×40 sccm
	Substrate temperature	T_S	RT, 120°C, 200°C
Process parameters	Discharge power	P	2–5 kW
	O_2 partial pressure	$p(O_2)$	$20 - 100$ mPa
	Ar partial pressure	$p(Ar)$	150 mPa
	Process control	-	$-P = f(p(O_2))$
	Substrate material	borosilicate glass AF45, Si	
	Deposition rate	a_s	$2–8\,nm\,s^{-1}$
	Film thickness	d	∼1,000 nm

The choice of the deposition parameters was based upon experiments on the reactive sputtering of transparent and conductive ZnO:X films [51, 68] described in the previous section. ZnO films with a thickness of $d \approx 1{,}000\,\mathrm{nm}$ were deposited at various reactive gas partial pressures onto unheated substrates and substrates at temperatures of 120 and 200°C.

Figure 5.13b shows the influence of the reactive gas partial pressure $p(O_2)$ on the deposition rate a during the reactive MF magnetron sputtering of ZnO coatings on quartz. The parameter space shows two regions, describing the growth of ZnO under an excess of either zinc or oxygen.

For growth under an excess of oxygen, an increase of the reactive gas partial pressure leads to a reduction in the deposition rate, which is independent of the substrate temperature. This results from the oxidization of the target, since the metallic particle current density $j(\mathrm{Zn})$ is reduced by the low sputtering yield of the oxidized target.

When film growth occurs under an excess of zinc, the influence of substrate temperature becomes significant. The expected steady decrease in deposition rate with increasing reactive gas partial pressure is only observed at low substrate temperatures – an increase in rate can already be seen at $T_\mathrm{S} = 200$°C when the reactive gas partial pressure is increased. As a first approximation, the deposition rate in this region is directly proportional to the reactive gas partial pressure, so that for $p(O_2) = 0\,\mathrm{mPa}$, no coating would result.

Qualitatively, this observation can be attributed to the high Zn vapor pressure. Once a critical substrate temperature is exceeded, sputtering at a low reactive gas partial pressure leads to the desorption of excess Zn, so the deposition rate is limited by the reactive gas partial pressure $p(O_2)$ as described earlier. Table 5.4 shows that the Zn vapor pressure at a substrate temperature of 300°C is still too low to explain the observed relationship. The Zn desorption is, however, supported by the intensive, high-energy ion bombardment of the MF excited magnetron discharge [38], so that desorption already takes place at lower substrate temperatures.

Similar relationships between the deposition rate, O_2 partial pressure, and substrate temperature have been noted in the literature [92]. Systematic investigations of the influence of ion bombardment on Zn desorption are reported in [93].

Figure 5.14 shows the X-ray diffraction patterns of ZnO films deposited at different substrate temperatures at $p(O_2) = 33\,\mathrm{mPa}$, where the maximum deposition rate is achieved. Only the (002) reflection of the wurtzite phase can be identified, which indicates textured growth of the polycrystalline films with the c-axis perpendicular to the substrate even at room temperature.

Table 5.4. Zn vapor pressure (from [91])

T	25	100	200	300
$p(\mathrm{Zn})$ (Pa)	2.5×10^{-8}	1.1×10^{-7}	7.3×10^{-4}	2.1×10^{-1}

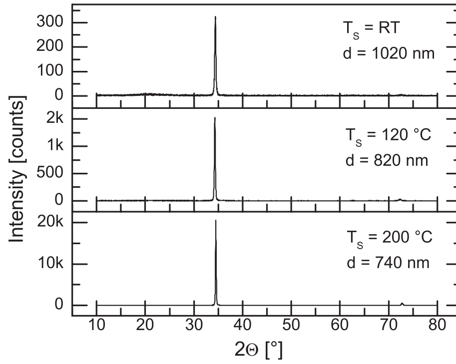

Fig. 5.14. XRD spectra measured in Bragg–Brentano geometry ($\Theta - 2\Theta$ or ω scans) for ZnO films deposited at the maximum rate ($p(O_2) = 33\,\mathrm{mPa}$) and different substrate temperatures

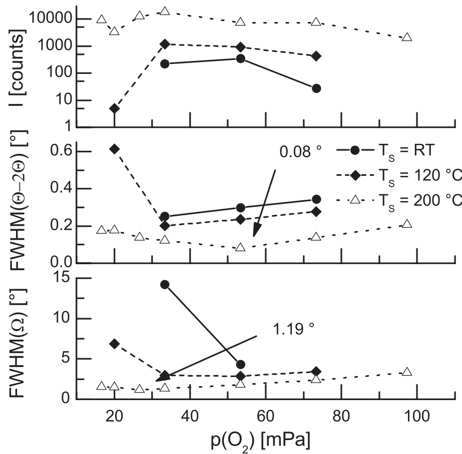

Fig. 5.15. (002) peak intensity I, full width at half maximum FWHM of the (002) peak and FWHM of the rocking curve as a function of oxygen partial pressure for three substrate temperatures

The intensity of the (002) reflections differs for films with comparable layer thickness by two orders of magnitude.

Figure 5.15 summarizes the analyses of the XRD measurements for the ZnO series deposited at different substrate temperature. The structural properties depend considerably on the substrate temperature and the reactive gas partial pressure. Films deposited at $T_S = 200°C$ in transition mode reveal the optimum properties.

From Figure 5.13b it follows that the transition between the two coating regimes takes place at a reactive gas partial pressure of $p(O_2) \approx 33\,\mathrm{mPa}$. At that partial pressure, the maximum rate is achieved for high substrate

temperatures. At low substrate temperatures, by contrast, the films are already fully transparent. The maximum rate at $T_S = 200°C$ is only 80% of the rate which is achieved for substrates at room temperature. The index of refraction measured at 550 nm using spectroscopic ellipsometry is between 2.03 and 2.04. The density is therefore similar. This indicates that the effect of Zn desorption is substantial for the high-temperature high-rate reactive magnetron sputtering of ZnO.

Figure 5.16 shows atomic force micrographs of samples deposited at $T_S = 200°C$ with different values of the reactive gas partial pressure $p(O_2)$ (minimum pressure, pressure corresponding to the maximum deposition rate and maximum pressure). The AFM micrographs reveal that the surface morphology for the samples deposited in the metallic mode and those deposited at the maximum rate is similar, whereas that of the samples deposited at high $p(O_2)$ is significantly different. For the sample deposited at $p(O_2) = 17$ mPa lateral structures about 100 nm in diameter, corresponding to coherently scattering crystallites, are noticeable. With the transition to a higher reactive gas partial pressure of $p(O_2) = 27$ mPa an increase of the crystallite size is visible, whereas the surface roughness decreases from 30.6 to 22.4 nm. The crystallites in these samples show predominantly circular boundaries. At $p(O_2) = 97$ mPa the layers are smooth, the RMS roughness is only 10.3 nm. For these samples long crystallites haphazardly arranged on the surface are observed, which overlap each other randomly (see the white arrow). The crystallites have a height of about 50 nm normal to the substrate (see arrow) and thus correlate with the grain size of 53 nm determined by XRD for these samples.

The transition in the morphology from $p(O_2) = 27$ mPa to $p(O_2) = 97$ mPa is due to reduced surface diffusion of Zn atoms under an excess of oxygen. At a high reactive gas partial pressure, the impinging species condense immediately, while at a lower reactive gas partial pressure the surface

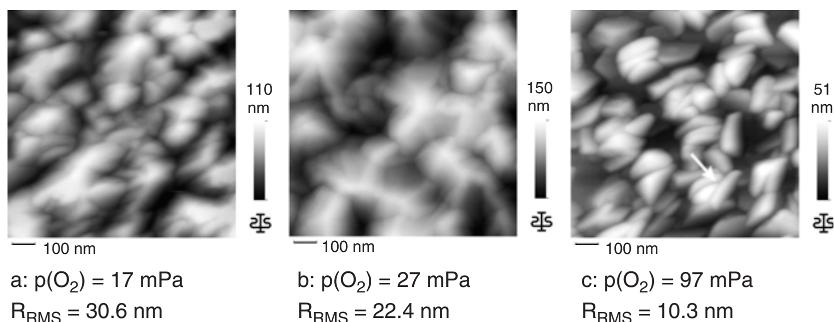

Fig. 5.16. AFM images ($1 \times 1\,\mu m^2$) of the surface morphology and root mean square value of the surface roughness R_{RMS} for 1 μm ZnO films deposited at $T_S = 200°C$ at different oxygen partial pressure

energy of the respective crystallites is minimized by surface diffusion of the Zn atoms, resulting in the formation of larger spherical aggregates.

Besides crystal orientation and surface morphology, the termination of the ZnO crystallites is another important parameter for the optimization of ZnO films: High piezo-electric coupling coefficients can only be achieved if the ZnO crystallites have a uniform polarity. There are only a few processes that allow the polarity of the ZnO films to be assessed.

For example, [94] reports a direct process for investigating ZnO polarity based on the analysis of time-of-flight spectra in ion-scattering experiments: low-energy ion beams are scattered over the surface of the layer, causing it to be sputtered by the ion bombardment. The detector allows the time-resolved detection of the Zn-particle stream and of the scattered primary ions. The extent of O termination and Zn termination for the layer can be calculated from the difference between these signals.

A simple process was used by Hickernell to determine polarity [3,95]: the criterion is the etching behavior of the ZnO layer since the $(00\bar{1})$-surface (O-terminated) shows an etching rate a factor of ten times greater than that of the (001)-surface (Zn-terminated). Perpendicular to the c-axis, the etching rate is 40–50 times the etching rate of the (001)-surfaces.

Good SAW (surface acoustic wave) characteristics are reported for Zn-terminated ZnO films homogeneously etched at low rates [95]. O-terminated crystallites lead to the development of craters which are identifiable in SEM (scanning electron microscopy) due to their higher etching rates.

Figure 5.17 compares SEM images of untreated and etched ZnO samples where etching has been performed for 5 s in 25% nitric acid at room temperature in an analogous manner to that reported by Hickernell [95]. In the untreated condition, a significant columnar structure is clearly recognizable in the breaking edge. The images of the etched samples show that almost no etching occurs at $p(O_2) = 17\,\text{mPa}$. At $p(O_2) = 20\,\text{mPa}$, on the other hand, the SEM reveals a rough surface morphology with deep etch craters. Etched samples deposited at higher oxygen partial pressure are not shown, since those films were fully etched away.

The conclusion in view of the results from Hickernell is that samples deposited at a low reactive gas partial pressure under Zn-excess conditions show a unique Zn termination, while the transition to deposition under oxygen excess leads to the development of O-terminated crystallites, so that for these samples unfavorable SAW characteristics are expected.

The transition mode process described here differs fundamentally from conventional reactive sputtering processes for ZnO coatings which do not permit optimization of the film characteristics since they are hysteresis-based. An example of this is the work of Jacobson et al. [96] on reactive DC-Magnetron sputtering of ZnO coatings.

The RF Magnetron sputtering of ceramic ZnO targets [97,98] offers fewer degrees of freedom for process optimization compared to the technology

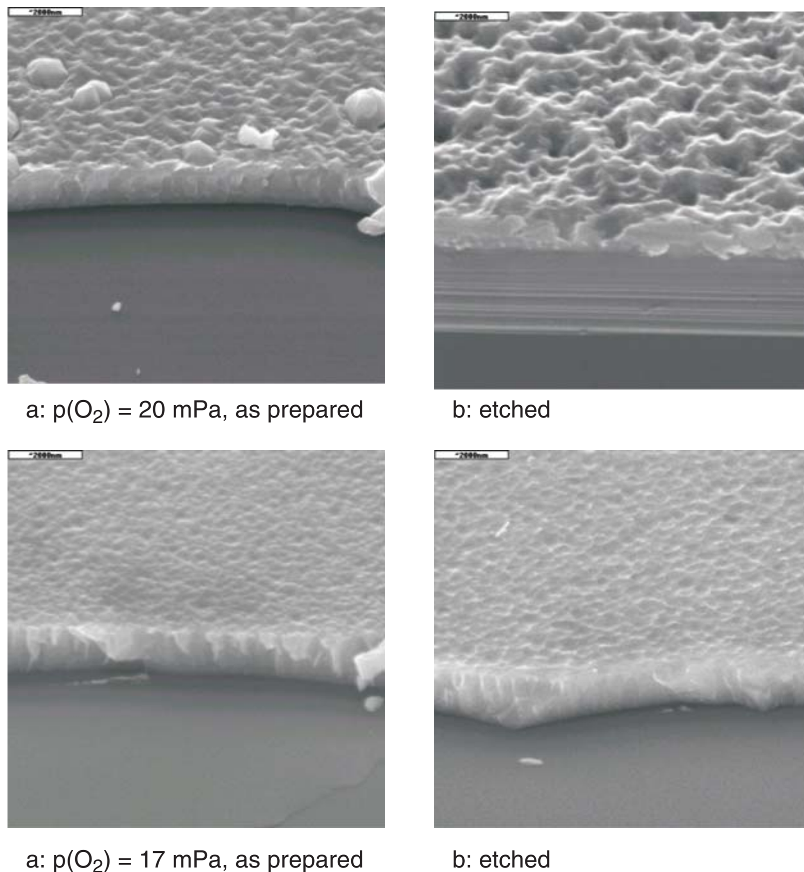

Fig. 5.17. SEM images of untreated and etched ZnO samples deposited under excess Zn conditions at $T_{\mathrm{S}} = 200°\mathrm{C}$

described here, because the advantageous deposition under Zn-excess conditions can be achieved only up to a certain extent due to the given stoichiometry of the ceramic target material.

The investigations described here show that the reactive MF magnetron sputtering of ZnO layer systems offers new degrees of freedom for process optimization, since the reactive gas partial pressure can be altered steadily even at high deposition rates. Films with high-quality structural characteristics were achieved particularly in the region of the unstable operating points that are not accessible with conventional reactive sputtering processes.

The ability to adjust the film-forming particle fluxes to the substrate continuously and to achieve plasma activation of the growth via ion bombardment from the plasma are key parameters for the deposition of doped ZnO films, as described in the subsequent sections.

Table 5.5. Literature survey of the structural data (FWHM of Bragg–Brentano-Scan and rocking curve) of ZnO layers for SAW applications

Process	T (°C)	FWHM ($\Theta - 2\Theta$) (°)	FWHM (Ω) (°)	Ref.
RMFMS	200	0.08	1.78	[90]
	200	0.14	1.19	[90]
RRFMS	590	0.22	2.85	[99]
	500	0.24		[4]
RFMS	300		1.77	[98]
RF-Mag-ECR	200	0.4	1.4	[100]
	300		2.9	[101]
PLD	350	0.13	2.07	[102]

RMFMS: reactive MF magnetron sputtering; RRFMS: reactive RF magnetron sputtering; RFMS: RF magnetron sputtering from a ceramic target; RF-Mag-ECR: RF magnetron mode ECR sputtering; PLD: pulsed laser deposition

Transparent Conductive Films

The transition mode process control described above is the key to reactive magnetron sputtering of ZnO:Al films. Several approaches have proven to be useful, either adjusting the reactive gas flow or the discharge power as a function of appropriate process variables.

As an example, Fig. 5.18 shows the dependence of film resistivity on oxygen partial pressure for the MF reactive magnetron sputtering of ZnO:Al films. The films were sputtered with the process control scheme described above for dielectric films (oxygen partial pressure measurement with a λ-sensor and adjustment of the discharge power). The process was implemented in an in-line coater using a dual cathode arrangement with 750 mm target length. Zn:2.0 wt% Al targets were used. Details are described in [103].

Substoichiometric films were obtained for $p(O_2) < 30$ mPa at low substrate temperatures up to $T_S = 180$°C. For higher substrate temperatures, Zn desorption occurs and thus, Al-rich films with poor electrical properties were grown with Al content up to 6%. At higher reactive gas partial pressure, constant dopant concentration is observed with $c_{Al} = 1.8 - 2.5$ at.%. For $p(O_2) = 30 - 35$ mPa, the films exhibit a low resistivity of $< 1{,}500\,\mu\Omega$ cm. For $T_S > 100$°C, films reveal resistivity of $\rho = 340 - 890\,\mu\Omega$ cm. At higher reactive gas partial pressure, excess reactive gas causes the oxidization of dopants and thus Al_2O_3 incorporation. These films show poor conductivity.

A compilation of the literature on transition mode process control for ZnO deposition is given within Table 5.1.

5.3.5 Ceramic Target Magnetron Sputtering

Ceramic target sputter processes utilize ceramic targets made by sintering or hot isostatic pressing (HIP). For lab-scale R&D work, another option is to use powder targets for sputtering [104].

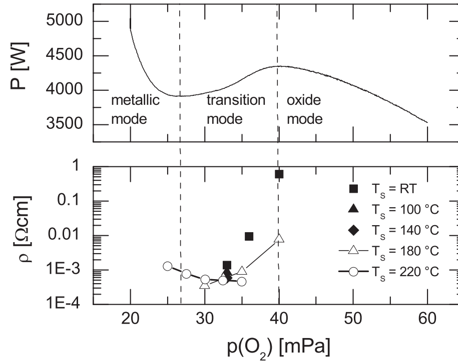

Fig. 5.18. Transition mode process stabilization and film resistivity for ZnO:Al films by reactive MF magnetron sputtering at different substrate temperature (reprinted from [103])

The main advantage of ceramic target sputtering is the fact that the oxygen for film formation is released from the target surface during sputtering. It is much easier to achieve stable deposition conditions since the difficult transition mode process control is not necessary. Furthermore, sputter processes from ceramic targets avoid the problem of Zn desorption when deposition is performed onto heated substrates. The main draw backs of ceramic target sputtering are the high costs for powder metallurgy and manufacturing of the ceramic targets.

RF sputtering is necessary when dielectric compounds such as sintered ZnO:Al_2O_3 disks are sputtered [58]. Since about 1995, it has been possible to make conductive sintered ceramics due to reducing annealing of the ceramic or due to incorporation of special dopants [80] on a large scale. When the conductivity of the target material is sufficient, it is possible to use either MF, pulsed, or DC plasma excitation for sputtering.

Properties such as high density and homogenous conductivity define the quality of ceramic targets. Ceramics with nonconductive inclusions exhibit arcing and nodule growth on the target surface, while targets with low density exhibit inferior film properties due to contaminations with different species.

Ceramic target magnetron sputtering has been used for fundamental materials development in several groups. The results from RF sputtering serve as a reference for the material properties that can be achieved by sputtering. ZnO:Al films with a resistivity as low as 140 cm were prepared by RF ceramic target magnetron sputtering at deposition rate of 1.2 nm min^{-1} at $T_S = 230°C$ [57].

The properties of ZnO:Al films for the application as the front electrode in a-Si:H p–i–n solar cells have been compared by Müller et al. [106].

A strong advantage from a process viewpoint is the fact that the Al enrichment for ZnO:Al films deposited by reactive magnetron sputtering at

Reactive sputtering	Ceramic targets	
Metallic targets	Sintered ZnO targets	HIP ZnO targets
Accurate process control required	Conventional DC- or Pulsed DC-Sputtering stable process	
Cheap alloy targets	Reasonable costs	Cost intensive production process
Excellent film properties are obtained with good control	Electrical properties not optimal	Film properties superior to sintered target

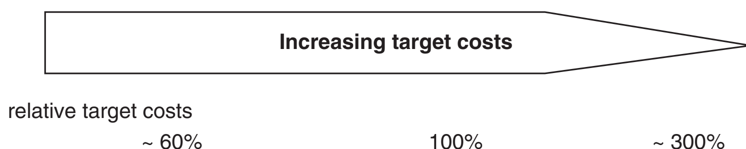

Fig. 5.19. Comparison of reactive and ceramic target sputtering processes. The relative target costs are a rough estimate for planar magnetron targets (from [105])

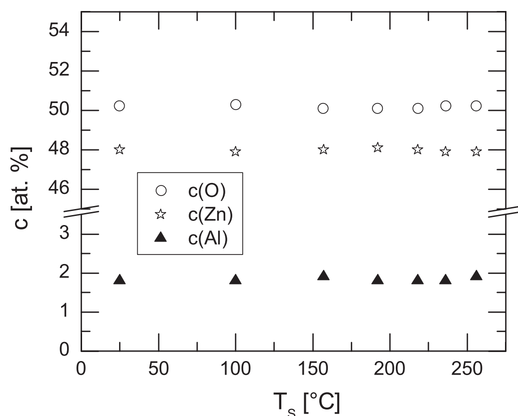

Fig. 5.20. Dependence of film composition of ZnO:Al films deposited by ceramic target magnetron sputtering on substrate temperature (from [107])

high temperature is not observed for ceramic target sputtering, as shown in Fig. 5.20 where no Al enrichment occurs for films deposited at substrate temperatures up to $T_S = 200°C$.

5.3.6 Other Technologies for Sputter Deposition of ZnO

The various magnetron sputter processes described above utilize the same plasma process for sputtering and for activating film growth on the substrate. There are also other techniques available, which permit a certain separation of sputtering and film growth activation.

The most prominent technique is ion beam sputtering, where one ion source is used for sputtering the target material and a second ion source may be used for activation of the film growth on the substrate surface. This approach allows precise adjustment of particle energy and particle fluxes to the substrate. Ion beam sputtering of ZnO-based films has been described in several publications [108–111]. The film properties of ion beam sputtered ZnO films are comparable to those obtained by magnetron sputtering. Nevertheless, industrial use of this technique is limited by the difficulty of up-scaling and the low deposition rate in the order of a few tens of nanometer per second.

Combining an electron cyclotron resonance (ECR) plasma with a sputtering process is another option to seperate sputtering and plasma activation. It has been shown to be an attractive technique for the deposition of dielectric ZnO films [101].

The combination of magnetron sputtering and inductively coupled plasma excitation (ICP) is a technique which allows enhanced ionization of the sputtered material. The combination of transition mode process control of the reactive sputtering and ICP plasma excitation is described in [112]. However, the resistivity of ZnO:Al films sputtered from a Zn:1.5 wt% Al target is in the of 1,000 µΩ cm at $T_\mathrm{S} = 150\,°\mathrm{C}$, which is inferior to results from conventional sputter processes under similar conditions.

5.4 Manufacturing Technology

5.4.1 In-Line Coating

The in-line manufacturing of ZnO-based TCO films is a highly efficient production technology, which has been adopted from the flat-panel display industry. Figure 5.21 shows a typical vertical in-line system used to deposit ZnO:Al over large areas for a-Si:H/µc-Si:H superstrate thin film photovoltaics by ceramic target or reactive magnetron sputtering.

For this application, a rough and well-defined surface morphology is necessary. It is achieved by post-deposition wet-chemical etching (see [113] and Chaps. 6 and 8). The film thickness to be deposited is in the order of 1,000 nm and about 300 nm of layer thickness is removed by the wet-chemical etching procedure.

A crucial parameter for the productivity of an in-line sputtering system is the cycle time, with the deposition rate of the magnetron sputter process being an important parameter. The film thickness d [nm] at a given substrate transport speed v_c [m min^{-1}] can be calculated from the dynamic deposition rate a_d [nm m min^{-1}] which is the film thickness when the substrate speed is 1 m min^{-1}. The dynamic rate can be derived from the static rate a_s [nm min^{-1}] on assuming the width b [m] of the coating zone.

$$d = a_\mathrm{d}/v_\mathrm{c} \quad \text{with} \quad a_\mathrm{d} = a_\mathrm{s} b$$

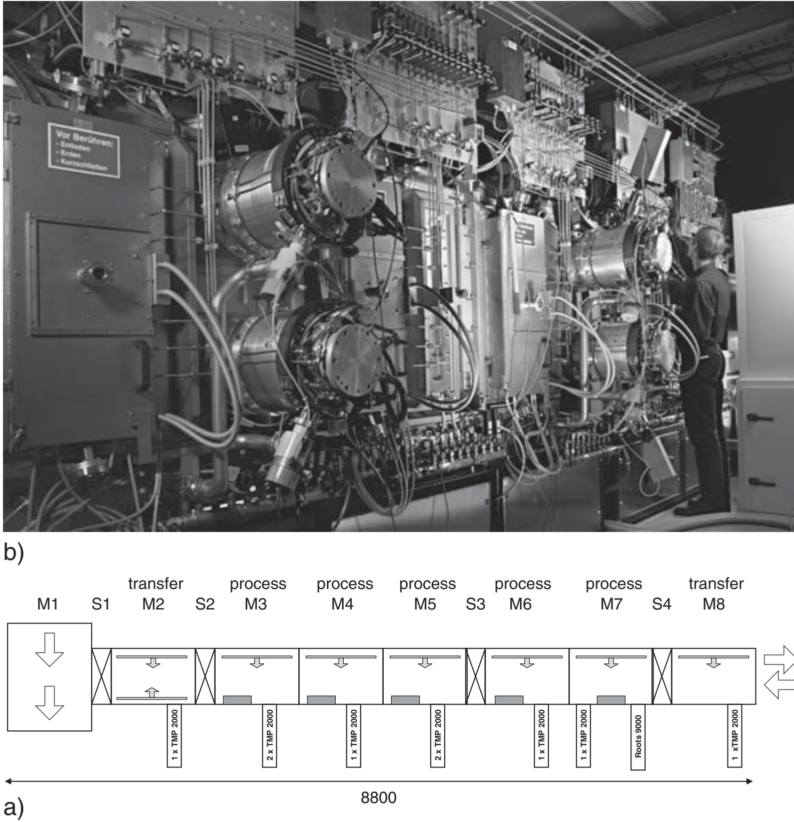

Fig. 5.21. Schematic diagram (from [103]) (**a**) and photo (**b**) of a large-area vertical in-line coater used for ZnO:Al-deposition (substrate dimensions up to $1{,}000 \times 600 \times 150 \times \mathrm{mm}^3$)

Dynamic deposition rates in the order of $60\,\mathrm{nm\,m\,min^{-1}}$ have been reported for dual magnetron reactive MF magnetron sputtering of high-quality ZnO:Al films at a moderate power density of $P/A \approx 4\,\mathrm{W\,cm^{-2}}$ [89]. In this case, the power density was limited by the power supply and the process control algorithms used. For an optimization towards higher deposition rates, dynamic deposition rates of $a_\mathrm{d} > 100\,\mathrm{nm \cdot m/min}$ can be reached [43]. The dependence of the dynamic rate and resistivity on total pressure and substrate temperature is shown in Fig. 5.22. It is important to notice the increase of the deposition rate at a high reactive gas partial pressure, which is due to the higher reaction efficiency and thus suppressed Zn desorption at higher oxygen partial pressure.

Similar deposition rates have been achieved using single magnetron ceramic target magnetron sputtering at high power density of $9\,\mathrm{W\,cm^{-2}}$. Sintered sputtering targets allow such high power densities even for long-term operation [80].

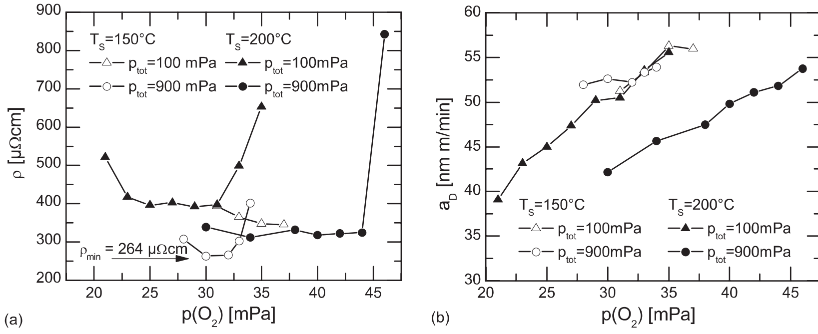

Fig. 5.22. Resistivity (**a**) and dynamic deposition rate (**b**) for large area reactive MF transition-mode magnetron sputtering at different total pressures and substrate temperatures. The power density is $\sim 4\,\mathrm{W\,cm^{-2}}$ (from [89])

5.4.1.1 Static Deposition

The deposition of ZnO coatings by in-line sputtering is basically a multilayer approach since the film grows under strongly varying conditions. The analysis of static deposition experiments in terms of particle flux and film property distribution is, therefore, helpful to understand and hence to improve the deposition process.

Coating by magnetron sputtering involves a variety of species impinging on the substrate. Low-energy bombardment (rough estimation: $E < 30\,\mathrm{eV}$) promotes the surface diffusion and enhances the reactivity of chemical species. High-energy particles, on the other hand, increase the film stress [114] and degrade the crystal structure, resulting in a high resistivity of the grown TCO film. The origin of the energetic flux is either the plasma sheath near the target (fast oxygen ions), the plasma sheath near the substrate (bombardment with positive ions), or the sputtering process itself (sputtered particles, reflected neutrals). As a consequence, the distribution of film properties may reveal quite substantial inhomogeneity.

Early work on the inhomogeneity of film properties was carried out by Tominaga et al. [116] and by Minami et al. [115]. Figure 5.23 shows the resistivity profile obtained for ZnO:Al ceramic target DC magnetron sputtering [115]. A low resistivity is observed for all temperatures in the center of the target. Opposite the racetrack, however, a high film resistivity is observed for substrate temperatures up to 325°C. At 350°C, on the other hand, the situation changed. The resistivity is homogenous due to the thermally induced healing of the crystal defects, which are caused by bombardment with fast oxygen ions.

Furthermore, the inhomogeneity due to the particle damage depends also on the erosion of the target used. This is shown in Fig. 5.24, where experiments with old and new targets have been compared [117, 118]. The new

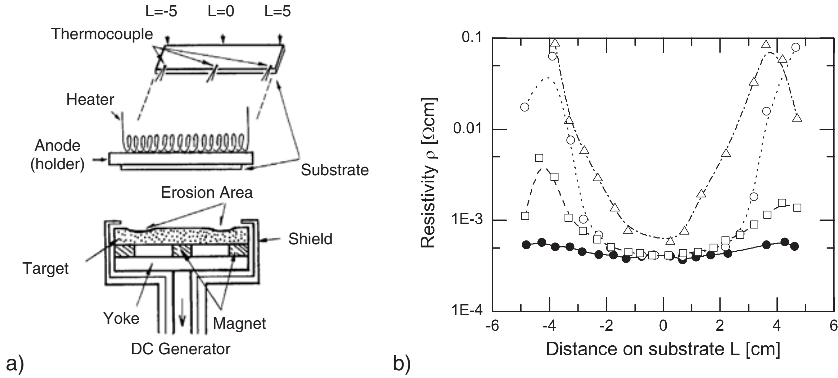

Fig. 5.23. Deposition system (**a**) and distribution of resistivity (**b**) for ZnO:Al film deposition by ceramic target (sintered ZnO:2.0 wt% Al_2O_3) DC magnetron sputtering. $T_S = 150°C$ (*open triangle*), 300°C (*open circle*), 325°C (*open square*) and 350°C (*bullet*) (reprinted from [115])

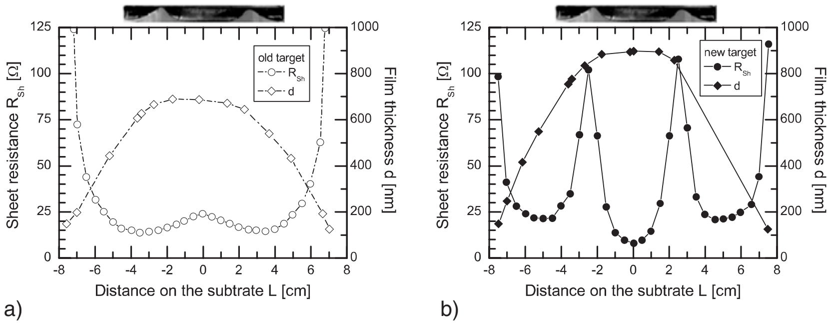

Fig. 5.24. Sheet resistance and film thickness distribution for static deposition DC magnetron sputtering of ZnO:Al on glass from sintered ZnO:Al_2O_3 targets using a new or an eroded sputtering target (reprinted from [117])

target exhibits a stronger effect since an intense oxygen ion particle beam is formed by the flat target surface.

In reactive magnetron sputtering, the situation is different since the formation of charged oxygen ions can be suppressed up to a certain extent by using an appropriate cathode configuration. Figure 5.25 shows a versatile layout for transition-mode dual magnetron sputtering which uses a plasma emission monitor to control the oxygen flow. The oxygen gas inlet connected to the piezo-electric valve is located between the targets, the sputter gas Ar is introduced via the outer gas lines. The experiment was intended to compare the resistivity profile when (1) all the reactive gas passes through the centeral gas inlet or when (2) a larger amount is introduced via the sputter gas inlet system.

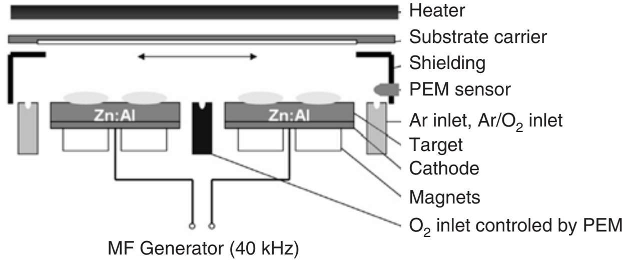

Fig. 5.25. Dual magnetron configuration for MF reactive magnetron transition-mode sputtering. Fast PEM control of the reactive gas flow inlet is applied via a piezoelectric valve for the gas inlet between the targets is used. Either all oxygen can be introduced between the cathodes or the total flow can be divided such that most of the reactive gas is introduced via the outer gas lines

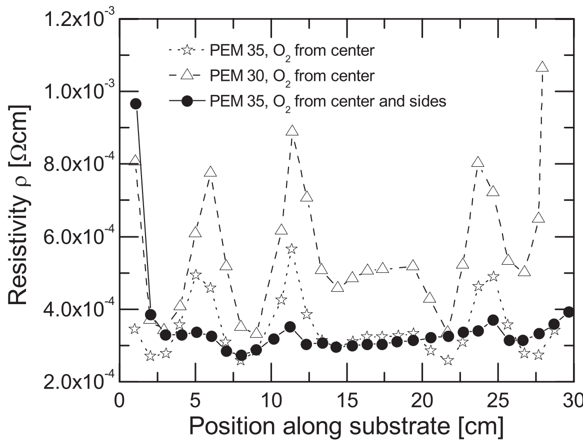

Fig. 5.26. Profile of resistivity obtained for static deposition using the configuration shown in Fig. 5.25

The resistivity profile observed is shown in Fig. 5.26. The well-known inhomogeneity is observed when the centeral gas inlet is used. Using the outer gas inlet to introduce some of the oxygen improves the resistivity considerably. Almost no damage due to energetic particles can be observed.

As a consequence, it must be emphasized that the generation of undesired high-energy species depends strongly on the configuration of the sputter system. Pressure gradients achieved by separated gas inlets may be useful for suppressing the formation of energetic oxygen ions. The ultimate goal is to prevent the interaction of oxygen with the high-density magnetron plasma near the target. One option to achieve this is to use ozone as the reactive gas directed toward the substrates. High sticking coefficients in the order of 100% have been reported for reactive DC magnetron sputtering of ITO using this approach [119].

5.4.1.2 Process Control

Achieving reproducible and homogenous film properties over large area substrates is a key requirement for industrial manufacturing. However, the conditions of the plasma discharge may vary over large area substrates since process perturbations are introduced during sputtering.

An important issue in in-line magnetron sputtering is the impact of the substrate transport on the pressure and plasma distribution. Appropriate conditions are achieved when the distance between the substrates in the coater is small (few centimeter). Under these conditions, the discrete substrates approximate a continuous ribbon and the impact of the substrate transport on the pressure distribution is small. In lab-scale or small-scale deposition systems, when only one carrier is passed through the system at a given time, the situation is non-ideal. The substrate transport gives rise to severe pressure changes, which can be modeled using direct simulation Monte-Carlo techniques [120]. A second issue is the desorption of adsorbents, in particular desorption of water, when substrates are transported into the vacuum system. These factors can be minimized by engineering the equipment appropriately.

The plasma process itself is subject to constant changes, at least due to the erosion of the target. In DC or pulsed magnetron sputtering using a single cathode, the anode is subject to coating. The build-up of dielectric films on the interior of the coater will therefore change the plasma configuration. The lack of process stability due to the disappearing anode effect is most critical for dielectric films such as SiO_2, but also has to be taken into account for sputtering of ZnO-based films.

The most sensitive issue, however, is the process stabilization of transition-mode reactive magnetron ZnO:Al sputtering for large substrates. For this application, it is not only mandatory to stabilize the reactive gas partial pressure at the center of the cathode. The second issue is to achieve symmetry control along the length of the targets, as the state of the targets may change due to local oxidization of the surface. This might occur on one end of the cathode, while the other end of the cathode operates still in the metallic mode.

An example of this problem is shown in Fig. 5.27, where the transition-mode closed-loop control of central oxygen partial pressure is performed by adjusting the discharge power. The graph shows that the central oxygen partial pressure is kept constant with high accuracy. Additional λ-sensors have been used to monitor the top and the bottom O_2 partial pressure. These pressures vary for the two consecutive runs by several millipascal. As a consequence, the films are neither homogeneous nor reproducible.

Therefore, the control loop shown in Fig. 5.28 was developed to solve the problem of symmetry control [121]. Two additional PID control loops are used to control the homogeneity of the reactive gas partial pressure because of appropriate regulation of the threefold gas inlet (top/center/bottom). The

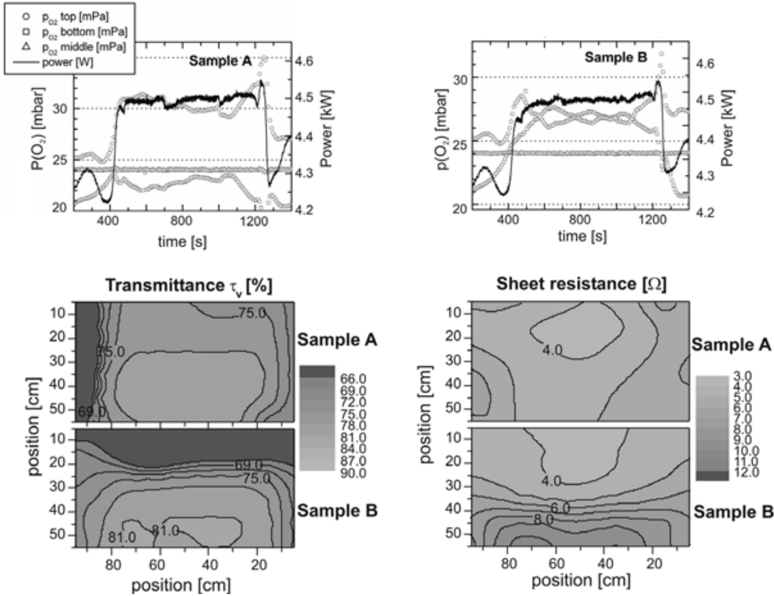

Fig. 5.27. Time dependence of the oxygen partial pressures and the discharge power during the coating process of substrates of 1,000 × 600 mm^2 using identical deposition conditions. Without symmetry control the oxygen partial pressures in the upper and lower part of the discharge may vary from one run to the next or change in an unpredictable manner during the process

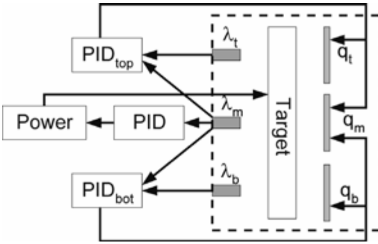

Fig. 5.28. Operating principal of the symmetry control for reactive MF magnetron sputtering of ZnO:Al. Three λ-sensors are used to monitor oxygen partial pressure at different positions along the target

measured $p(O_2)$ values are used as input for a control loop controlling the threefold oxygen inlet.

An example for the performance of the control loop is shown in Fig. 5.29, where changes of $p(O_2)$ and $p(\mathrm{tot})$ have been made. Due to the symmetry control, it was possible to achieve constant $p(O_2)$ over the length of the cathodes.

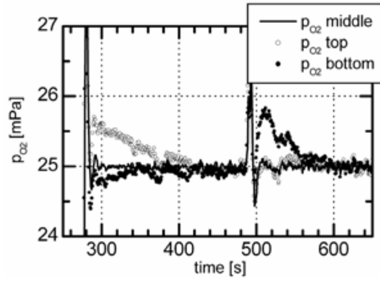

Fig. 5.29. Example of the response of the control loop to perturbations such as a changed setting for $p(O_2)$ at 280 s or a change of total pressure in the chamber (at 500 s) for statistic deposition. The symmetry control was set to equalize the partial pressures at all three positions

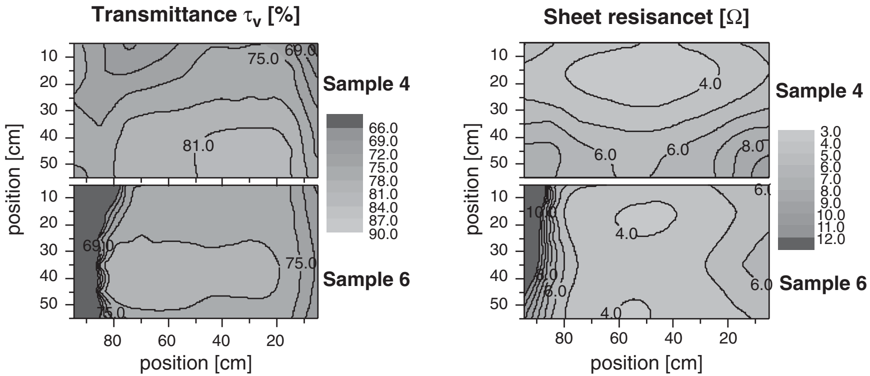

Fig. 5.30. Optical transmittance and sheet resistivity of samples deposited under identical deposition conditions with active symmetry control. The highly absorbing region on sample 6 (entrance region) is an artefact due to incorrect positioning of the carrier

The impact of symmetry control on the homogeneity of film properties for large-area ZnO:Al coating is shown in Fig. 5.30. Homogeneous coatings with acceptable variation of transmittance and sheet resistance have been achieved. The concept of symmetry control described here is well known in the glass industry. Other implementations have been realized using multiple PEM sensors [43].

5.4.2 Rotatable Target Magnetron Sputtering

The concept of rotatable target magnetron (C-Mag) sputtering is shown in Fig. 5.31a. The target material is a water-cooled tube, which is attached to

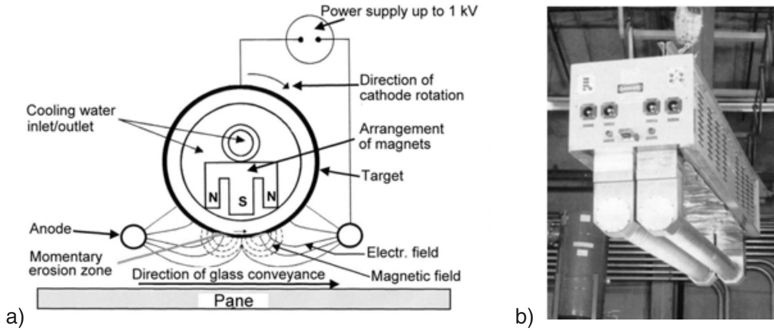

Fig. 5.31. (**a**) Cross-section (reprinted from [123]) and industrial construction (**b**) of rotatable magnetron sputter sources

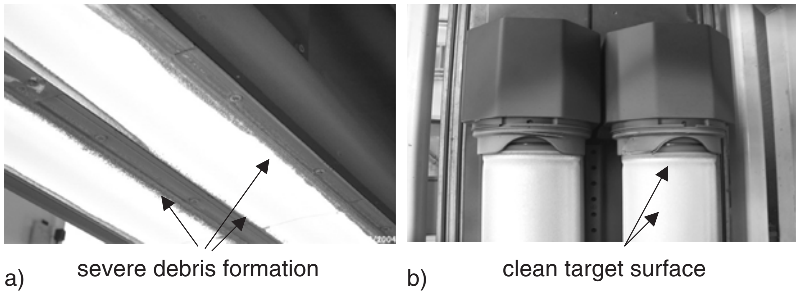

Fig. 5.32. Photographs of double magnetron planar (**a**) and rotatable (**b**) targets after long-term reactive sputtering of ZnO:Al. The planar target is shown after 1,850 kW h, the rotatable target after 11,500 kW h (source: Von Ardenne Anlagentechnik, Dresden)

the end blocks containing the sealing, the water and power feedthroughs and the rotary drive [122].

A key advantage of ZnO C-Mag sputtering is the decrease of debris and defect formation since the target rotates, so that the redeposition zones on the target are sputtered continuously. Figure 5.32 compares the target surface for planar and rotatable reactive magnetron sputtering of ZnO:Al. Severe formation of debris occurs on the surfaces of the planar cathodes, while there is no debris on the rotatable target. Similarly, redeposition zones can be prevented by using planar magnetrons with moving magnets [89].

Further advantages are the higher degree of material utilization and the large material stock, which is raised by a factor of 4 compared with planar targets. Both factors enable long-term operation (up to 2 weeks uninterrupted) without maintenance, while planar cathodes have to be maintained each week.

5.5 Emerging Developments

5.5.1 Ionized PVD Techniques

Process techniques such as filtered arc [124–126] deposition, or pulsed laser deposition [79, 127–130] generate outstanding film properties for a variety of TCO materials. The main feature is that the film formation is achieved with ions instead of using mostly neutral atoms. The state of the art is the pulsed laser deposition of ZnO:Al films, where resistivity of 85 $\mu\Omega$ cm has been reported at a substrate temperature of 230°C [79]. This result can be attributed to the high doping efficiency because of the suppression of Al_2O_3 formation when ionized species are used for film formation.

The new concept of high-power pulsed magnetron sputtering (HPPMS) allows for similar plasma characteristics using large-area magnetron sputtering [131]. Power densities in the order of 1 kW cm^{-2} are applied in short pulses. This mode of operation leads to a substantial ionization of the sputtered material. Ionization on the order of 80% has been shown for Ag sputtering. ITO films deposited by HPPMS have shown improved performance compared with conventional sputtering in terms of surface morphology and resistivity [132]. For ZnO:Al, the relevant parameter space has not been achieved up to now due to unstable process caused by arcing at high levels of ionization. However, initial promising results have been reported for room temperature deposition of ZnO:Al using reactive HPPMS [133].

5.5.2 Hollow Cathode Sputtering

Hollow cathode gas flow sputtering is an alternative approach for large-area sputter deposition of oxides. A schematic diagram of the hollow cathode gas flow sputter process is shown in Fig. 5.33. A hollow cathode glow discharge with high plasma density is formed between the targets. The sputtered material is transported to the substrate in an Ar flow via forced convection. Reactive gas is introduced in the afterglow region of the discharge in a way that the metallic mode operation of the targets is not disturbed.

Hollow cathode gas flow sputtering operates in the pressure range of 0.1–1 mbar. The particles are thermalized at the substrate. Plasma activation of growth processes can be achieved either by applying a substrate bias or by pulsed mode operation of the discharge.

Hollow cathode gas flow sputtering is a promising technique for gentle growth of ZnO films on sensitive substrate materials (e.g., organic photovoltaics and OLEDs). Furthermore, the process can be operated as a PVD/PECVD hybrid process for organic modification of ceramic films. The third process regime is the deposition of nanoparticles, since clusters are formed in the gas phase in high-pressure and high-power regime [134].

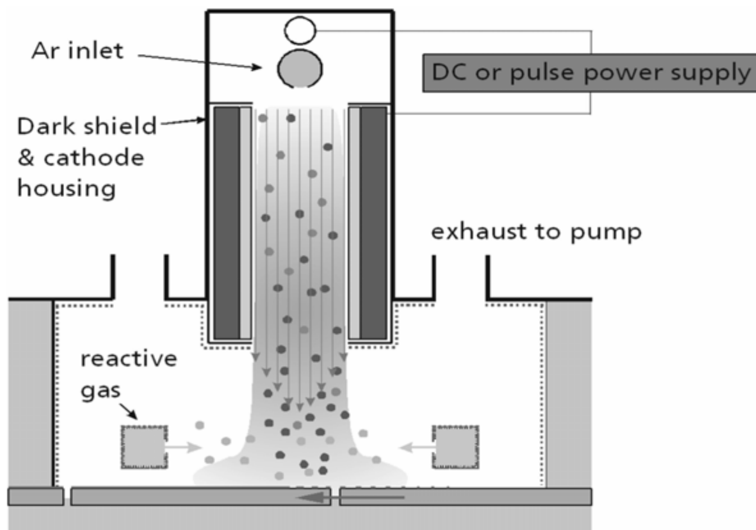

Fig. 5.33. Schematic diagram of hollow cathode gas flow sputtering. Total pressure: $p_{\mathrm{tot}} \approx 0.1 - 1\,\mathrm{mbar}$. Gas flow: $q(\mathrm{Ar}) \approx 1 - 5\,\mathrm{slm}$ for 75 cm target length

5.5.3 Model-Based Process Development

Understanding the dependence of film structure and morphology on system layout and process parameters is a core topic for the further development of ZnO technology. Work is being performed on in situ characterization of deposition processes. Growth processes are simulated using Direct Simulation Monte-Carlo (DSMC) techniques to simulate the gas flow and sputter kinetics simulation and Particle-In-Cell Monte-Carlo (PICMC) techniques for the plasma simulation [132].

An example is given in Fig. 5.34, where a photo of a MF sputter process taken with a high speed camera is shown in comparison to the corresponding simulation of plasma density. The right-hand target is shown in cathode operation, while the left-hand target serves as the anode. The plasma is confined between the targets. The anode is shielded by the magnetron's magnetic field and thus, the plasma reaches the anode in the area between the racetracks where the magnetic field is weak. The racetrack area itself is subject only to a weak electron current drawn from the plasma. This explains why arcing is still observed in dual magnetron MF sputtering to some extent, in contrast to early models, which predicted that some 10 kHz of plasma excitation should be sufficient to prevent arcing.

Acknowledgements. The work presented here was supported by the German Ministry for Science and Education (BMBF) within the framework of the OSTec project on development of energy-efficient glazing (project No. 13N6520), the ZnO network project (project No. 01SF00314) and the 2+2 project transparent conductive

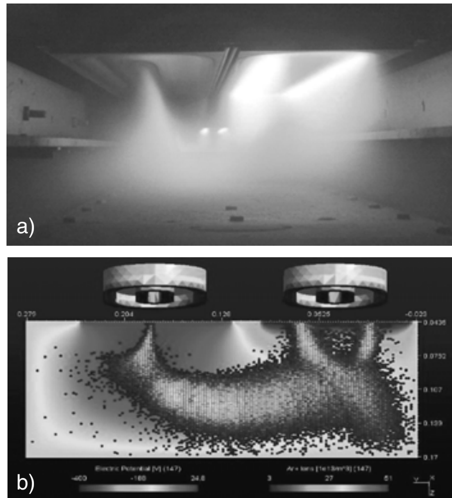

Fig. 5.34. (**a**) High-speed photograph (source: Fraunhofer FEP, Dresden) and (**b**) plasma simulation of an MF magnetron in-line sputter process (source: Fraunhofer IST, Braunschweig)

oxide films (project No. NMT/03X2303A). The work would not have been possible without the constantly stimulating discussions and the fruitful cooperation of the project partners. I acknowledge the strong commitment of my coworkers Prof. Dr. Xin Jiang, Dr. Volker Sittinger, Dr. Rujang Hong, and Florian Ruske to the success of our work. Furthermore, I also thank Thomas Höing, Udo Bringmann, Ralf Pöckelmann, Claudia Jacobs, André Kaiser, and Wolfgang Werner for various discussions and their outstanding support in the course of the projects.

References

1. J.S. Chapin, Res. Dev. **25**, 37 (1974)
2. F.S. Hickernell, J. Appl. Phys. **44**, 1061 (1973)
3. F.S. Hickernell, Rev. Phys. Appl. **20**, 319 (1985)
4. F.C.M. van de Pol, F.R. Blom, T.J.A. Popma, Thin Solid Films **204**, 349 (1991)
5. H.J. Gläser, Glass Technol. **21**, 254 (1980)
6. R.E. Laird, J.D. Wolfe, SVC Ann. Tech. Conf. Proc. **37**, 428 (1994)
7. M. Arbab, Thin Solid Films **381**, 15 (2001)
8. Y. Tsuda, H. Omoto, K. Tanaka, H. Ohsaki, Thin Solid Films **502**, 223 (2006)
9. J. Kawaguchi, E. Kusano, Patent de 3628057a1, 1986
10. M.J. Brett, R.W. McMahon, J.D. Affinito, R. Parsons, J. Vac. Sci. Technol. A **1**, 352 (1983)
11. K. Ellmer, F. Kudella, R. Mientus, R. Schieck, S. Fiechter, Thin Solid Films **247**, 15 (1994)

12. R. Menner, R. Schäffler, B. Sprecher, B. Dimmler, in *Proceedings of the 2nd World Conference on Photovoltaic Energy Conversion*, Vienna, 1998
13. J. Müller, G. Schöpe, O. Kluth, B. Rech, V. Sittinger, B. Szyszka, R. Geyer, P. Lechner, H. Schade, M. Ruske, G. Dittmar, H.-P. Bochem, Thin Solid Films **442**, 158 (2003)
14. R.K. Waits, J. Vac. Sci. Technol. **15**, 179 (1978)
15. R.K. Waits, J. Vac. Sci. Technol. A **18**, 1736 (2000)
16. D.M. Mattox, SVC Ann. Tech. Conf. Proc. **47**, 23 (2004)
17. R. Latz, K. Michael, M. Scherer, Jpn. J. Appl. Phys. **30**, L149 (1991)
18. M. Katayama, Thin Solid Films **341**, 140 (1999)
19. P. Binkowska, B. Cord, P. Wohlfart, Microsyst. Technol. **13**, 139 (2007)
20. J. Schroeder, B. Cord, W. Maaß, K.H. Schuller, U. Patz, Thin Solid Films **175**, 287 (1989)
21. J.S. Colligon, J. Vac. Sci. Technol. A **13**, 1649 (1995)
22. D.W. Hess, J. Vac. Sci. Technol. A **8**, 1677 (1990)
23. N. Kaiser, Appl. Opt. **41**, 3053 (2002)
24. J.A. Thornton, Surface Eng. **2**, 283 (1986)
25. P.J. Kelly, R.D. Arnell, Vacuum **56**, 159 (2000)
26. R. Herrmann, G. Bräuer, in *Thin Films for Optical Coatings*, ed. by R.E. Hummel, K.H. Guenter. Handbook of Optical Properties, vol. 1 (CRC, Boca Raton, 1995) pp. 135–187
27. B. Chapman, *Glow Discharge Processes* (Wiley, New York, 1980)
28. Y.P. Raizer, *Gas Discharge Physics* (Springer, Berlin Heidelberg New York, 1991)
29. D. Rosen, I. Katardjiev, S. Berg, W. Möller, Nucl. Instrum. Meth. B **228**, 193 (2005)
30. S.M. Rossnagel, in *Handbook of Vacuum Science and Technology*, ed. by D. Hoffman, B. Singh, J. Thomas (Academic Press, San Diego, 1998) pp. 609–627
31. R. Behrisch (ed.), *Sputtering by Particle Bombardment I* (Springer, Berlin Heidelberg New York, 1981)
32. R. Behrisch (ed.), *Sputtering by Particle Bombardment II* (Springer, Berlin Heidelberg New York, 1983)
33. R.E. Somekh, J. Vac. Sci. Technol. A **2**, 1285 (1984)
34. T. Takagi, J. Vac. Sci. Technol. A **2**, 382 (1984)
35. H.J. Gläser (ed.), Large Area Glass Coating (Von Ardenne Anlagentechnik GmbH, Dresden, 2002)
36. F.M. Penning, U.S. Patent 2,146,025, 1936
37. F.M. Penning, J.H. Moubis, Proc. K. Ned. Akad. Wet. **43**, 203 (1940)
38. S. Jäger, B. Szyszka, J. Szczyrbowski, G. Bräuer, Surf. Coat. Technol. **98**, 1304 (1998)
39. R. Cebulla, R. Wendt, K. Ellmer, J. Appl. Phys. **83**, 1087 (1998)
40. G.L. Harding, B. Window, E.C. Horrigan, Sol. Energ. Mater. **22**, 69 (1991)
41. M.J. Brett, R.R. Parsons, Solid State Commun. **54**, 603 (1985)
42. S. Brehme, F. Fenske, W. Fuhs, E. Nebauer, M. Poschenrieder, B. Selle, I. Sieber, Thin Solid Films **342**, 167 (1999)
43. T. Wallendorf, S. Marke, C. May, J. Strümpfel, Surf. Coat. Technol. **174–175**, 222 (2003)
44. H. Czternastek, A. Brudnik, M. Jachimowski, E. Kolawa, J. Phys. D Appl. Phys. **25**, 865 (1992)

45. T. Nakada, Y. Ohkubo, A. Kunioka, Jpn. J. Appl. Phys. **30**, 3344 (1991)
46. T. Minami, K. Oohashi, S. Takata, T. Mouri, N. Ogawa, Thin Solid Films **193–194**, 721 (1990)
47. M. Miyazaki, K. Sato, A. Mitsui, H. Nishimura, J. Non-Cryst. Solids **218**, 323 (1997)
48. M. Kon, P.K. Song, A. Mitsui, Y. Shigesato, Jpn. J. Appl. Phys. **41**, 6174 (2002)
49. T. Minami, T. Yamamoto, T. Miyata, Thin Solid Films **366**, 63 (2000)
50. N. Malkomes, M. Vergöhl, B. Szyszka, J. Vac. Sci. Technol. A **19**, 414 (2001)
51. B. Szyszka, Thin Solid Films **351**, 164 (1999)
52. M. Kon, P.K. Song, Y. Shigesato, P. Frach, S. Ohno, K. Suzuki, Jpn. J. Appl. Phys. **42**, 263 (2003)
53. Y. Igasaki, M. Ishikawa, G. Shimaoka, Appl. Surf. Sci. **33–34**, 926 (1988)
54. J.B. Webb, D.F. Williams, M. Buchanan, Appl. Phys. Lett. **39**, 640 (1981)
55. T. Minami, H. Nanto, S. Takata, Appl. Phys. Lett. **41**, 958 (1982)
56. K. Ito, T. Nakazawa, Jpn. J. Appl. Phys. **22**, 245 (1983)
57. Y. Igasaki, H. Saito, J. Appl. Phys. **70**, 3613 (1991)
58. S. Bose, S. Ray, A.K. Barua, J. Appl. Phys. **29**, 1873 (1996)
59. R. Wang, L.L.H. King, A.W. Sleight, J. Mater. Res. **11**, 1659 (1996)
60. T. Minami, H. Sato, H. Nanto, S. Takata, Jpn. J. Appl. Phys. **24**, L781 (1985)
61. K.C. Park, D.Y. Ma, K.H. Kim, Thin Solid Films **305**, 201 (1997)
62. M.L. Addonizio, A. Antonaia, G. Cantele, C. Privato, Thin Solid Films **349**, 93 (1999)
63. F.-J. Haug, Z. Geller, H. Zogg, A.N. Tiwari, C. Vignali, J. Vac. Sci. Technol. A **19**, 171 (2001)
64. B.H. Choi, H.B. Im, J.S. Song, K.H. Yoon, Thin Solid Films **193**, 712 (1990)
65. Z.C. Jin, I. Hamberg, C.G. Granqvist, Thin Solid Films **164**, 381 (1988)
66. W.D. Westwood, in *Physics of Thin Films*, vol. 14, ed. by M.H. Fracombe, J.L. Vossen (Academic Press, New York, 1989) pp. 1–79
67. S. Schiller, G. Beister, W. Sieber, Thin Solid Films **111**, 259 (1984)
68. B. Szyszka, Ph.D. thesis, Justus-Liebig-Universität (1999)
69. C. Nender T. Larsson, H.O. Blomm, S. Berg, J. Vac. Sci. Technol. A **6**, 1832 (1988)
70. S. Berg, T. Nyberg, Thin Solid Films **476**, 215 (2005)
71. N. Malkomes, M. Vergöhl, J. Appl. Phys. **89**, 732 (2001)
72. V. Kirchhoff, T. Kopte, T. Winkler, M. Schulze, P. Wiedemuth, Surf. Coat. Technol. **98**, 828 (1998)
73. H. Kupfer, R. Kleinhempel, F. Richter, C. Peters, U. Krause, T. Kopte, Y. Cheng, J. Vac. Sci. Technol. A **24**, 106 (2006)
74. D.J. Christie, H.V. Walde, T.J. Ash, SVC Ann. Tech. Conf. Proc. **48**, 39 (2005)
75. J. Szczyrbowski, G. Teschner, SVC Ann. Tech. Conf. Proc. **38**, 389 (1995)
76. G. Bräuer, M. Ruske, J. Szczyrbowski, G. Teschner, A. Zmelty, Vacuum **51**, 655 (1998)
77. J. Aranovich, A. Ortiz, R.H. Bube, J. Vac. Sci. Technol. A **16**, 994 (1979)
78. T. Minami, H. Sato, H. Nanto, S. Takata, Thin Solid Films **176**, 277 (1989)
79. H. Agura, A. Suzuki, T. Matsushita, T. Aoki, M. Okuda, Thin Solid Films **445**, 263 (2003)
80. F. Ruske, V. Sittinger, W. Werner, B. Szyszka, K. Dietrich, R. Rix, K. U. van Osten, Surf. Coat. Technol. **200**, 236 (2005)

81. C.G. Van de Walle, Phys. Rev. Lett. **85**, 1012 (2000)
82. S. Maniv, C.J. Miner, W.D. Westwood, J. Vac. Sci. Technol. A **1**, 1370 (1983)
83. R. Wendt, K. Ellmer, Surf. Coat. Technol. **93**, 27 (1997)
84. N. Malkomes, B. Szyszka, J. Vac. Sci. Technol. A **19**, 2368 (2001)
85. M. Vergöhl, N. Malkomes, T. Matthée, G. Bräuer, Thin Solid Films **377–378**, 43 (2000)
86. N. Malkomes, A. Pflug, B. Szyszka, M. Vergöhl, SVC Ann. Tech. Conf. Proc. **45**, 41 (2002)
87. W.D. Sproul, D.J. Christie, D.C. Carter, Thin Solid Films **491**, 1 (2005)
88. C. May, R. Menner, J. Strümpfel, M. Oertel, B. Sprecher, Surf. Coat. Technol. **169–170**, 512 (2003)
89. B. Szyszka, V. Sittinger, X. Jiang, R.J. Hong, W. Werner, A. Pflug, M. Ruske, A. Lopp, Thin Solid Films **442**, 179 (2003)
90. B. Szyszka, Thin Solid Films, submitted
91. O. Kubaschewski, C.B. Alcock, *Metallurgical Thermochemistry* (Pergamon, Oxford, 1979)
92. N. Tsuji, H. Komiyama, K. Tanaka, Jpn. J. Appl. Phys. **9**, 835 (1990)
93. M.J. Brett, R.R. Parsons, Can. J. Phys. **63**, 819 (1985)
94. T. Ohnishi, A. Ohtomo, K. Takahashi, M. Yoshimoto, H. Koinuma, Appl. Phys. Lett. **72**, 824 (1998)
95. F.S. Hickernell, T. Hickernell, in *IEEE Ultrasonics Symposium*, 373–376, 1992
96. E. Jacobsohn, D. Shechtman, Mat. Res. Soc. Symp. Proc. **242**, 779 (1992)
97. K.B. Sundaram, A.I. Khan, Thin Solid Films **295**, 87 (1997)
98. S. Takada, J. Appl. Phys. **73**, 4739 (1993)
99. J.G. Gardeniers, Z.M. Rittersma, G.J. Burger, J. Appl. Phys. **83**, 7844 (1998)
100. M. Kadota, M. Minakata, Jpn. J. Appl. Phys. **37**, 2923 (1998)
101. T. Inukai, M. Matsuoka, K. Ono, Thin Solid Films **257**, 22 (1995)
102. V. Craciun, J. Elders, J.G. Gardeniers, I.W. Boyd, Appl. Phys. Lett. **65**, 2963 (1994)
103. B. Szyszka, T. Höing, X. Jiang, A. Bierhals, N. Malkomes, M. Vergöhl, V. Sittinger, U. Bringmann, G. Bräuer, SVC Ann. Tech. Conf. Proc. **44**, 272 (2001)
104. P.J. Kelly, Y. Zhu, A. Postill, Thin Solid Films **426**, 111 (2003)
105. K.U. van Osten, (gfe) company information, 2007
106. J. Müller, G. Schöpe, O. Kluth, B. Rech, M. Ruske, J. Trube, B. Szyszka, X. Jiang, G. Bräuer, Thin Solid Films **392**, 327 (2001)
107. F. Ruske, Ph.D. thesis, Justus-Liebig-Universität (2007)
108. Y. Qu, T.A. Gessert, K. Ramanathan, R.G. Dhere, R. Noufi, T.J. Coutts, J. Vac. Sci. Technol. A **11**, 996 (1993)
109. Y. Qu, T.A. Gessert, T.J. Coutts, R. Noufi, J. Vac. Sci. Technol. A **12**, 1507 (1994)
110. S. Kohiki, M. Nishitani, T. Wada, Jpn. J. Appl. Phys. **33**, 6706 (1994)
111. J.W. Seong, K.-H. Kim, Y.W. Beag, S.K. Koh, K.H. Yoon, J. Vac. Sci. Technol. A **22**, 1139 (2004)
112. S.J. Jung, Y.H. Han, B.M. Koo, J.J. Lee, J.H. Joo, Thin Solid Films **475**, 275 (2005)
113. B. Rech, O. Kluth, T. Repmann, T. Roschek, J. Springer, J. Müller, F. Finger, H. Stiebig, H. Wagner, Sol. Energ. Mater. Sol. Cell. **74**, 439 (2002)
114. H. Windischmann, Crit. Rev. Solid State **17**, 547 (1992)

115. T. Minami, H. Sato, H. Imamoto, S. Takata, Jpn. J. Appl. Phys. **31**, 257 (1992)
116. K. Tominaga, T. Yuasa, M. Kume, O. Tada, Jpn. J. Appl. Phys. **24**, 944 (1985)
117. R. Mennerm, M. Powalla, in *Forschungsverbund Sonnenenergie Tagungsband*, 71–78, 2005
118. D. Severin, O. Kappertz, T. Nyberg, S. Berg, M. Wuttig, Thin Solid Films **515**, 3554 (2007)
119. A. Alam, K. Sasaki, T. Hata, Thin Solid Films **281**, 209 (1996)
120. A. Pflug, N. Malkomes, V. Sittinger, B. Szyszka, SVC Ann. Tech. Conf. Proc. **45**, 16 (2002)
121. F. Ruske, A. Pflug, V. Sittinger, W. Werner, B. Szyszka, Thin Solid Films **502**, 44 (2006)
122. J. Rietzel, S. Nadel, SVC Ann. Tech. Conf. Proc. **47**, 224 (2004)
123. M.W. McBride, SVC Ann. Tech. Conf. Proc. **33**, 250 (1990)
124. A. Ben-Shalom, L. Kaplan, R.L. Boxman, S. Goldsmith, M. Nathan, Thin Solid Films **236**, 20 (1993)
125. L. Kaplan, A. Ben-Shalom, R.L. Boxman, S. Goldsmith, U. Rosenberg, M. Nathan, Thin Solid Films **253**, 1 (1994)
126. T. David, S. Goldsmith, R.L. Boxman, Thin Solid Films **447–448**, 61 (2004)
127. A. Suzuki, T. Matsushita, N. Wada, Y. Sakamoto, M. Okuda, Jpn. J. Appl. Phys. **35**, L56 (1996)
128. H. Hiramatsu, K. Imaeda, N. Horio, M. Nawata, J. Vac. Sci. Technol. A **16**, 669 (1998)
129. H. Hosono, H. Ohta, M. Orita, K. Ueda, M. Hirano, Vacuum **66**, 419 (2002)
130. H. Tanaka, K. Ihara, T. Miyata, H. Sato, T. Minami, J. Vac. Sci. Technol. A **22**, 1757 (2004)
131. U. Helmersson, M. Lattemann, J. Bohlmark, A.P. Ehiasarian, J.T. Gudmundsson, Thin Solid Films **513**, 1 (2006)
132. M. Siemers, A. Pflug, B. Szyszka, SVC Ann. Tech. Conf. Proc. **49**, 60 (2006)
133. F. Ruske, A. Pflug, V. Sittinger, W. Werner, B. Szyszka, D.J. Christie, in *Proceedings of the 6th International Conference on Coatings on Glass and Plastics*, Dresden, Germany, 2006
134. M. Birkholz, U. Albers, T. Jung, Surf. Coat. Technol. **179**, 279 (2004)